JOURNAL OF GEOPHYSICAL RESEARCH, VOL. 107, NO. B1, 2005, 10.1029/2001JB000355, 2002

Control of folding by gravity and matrix thickness: Implications for large-scale folding

S. M. Schmalholz,[1] Y. Y. Podladchikov, and J.-P. Burg
Geologisches Institut, ETH Zentrum, Zürich, Switzerland

Received 27 June 2000; revised 8 May 2001; accepted 9 June 2001; published 8 January 2002.

[1] We show that folding of a non-Newtonian layer resting on a homogeneous Newtonian matrix with finite thickness under influence of gravity can occur by three modes: (1) matrix-controlled folding, dependent on the effective viscosity contrast between layer and matrix, (2) gravity-controlled folding, dependent on the Argand number (the ratio of the stress caused by gravity to the stress caused by shortening), and (3) detachment folding, dependent on the ratio of matrix thickness to layer thickness. We construct a phase diagram that defines the transitions between each of the three folding modes. Our priority is transparency of the analytical derivations (e.g., thin-plate versus thick-plate approximations), which permits complete classification of the folding modes involving a minimum number of dimensionless parameters. Accuracy and sensitivity of the analytical results to model assumptions are investigated. In particular, depth dependence of matrix rheology is only important for folding over a narrow range of material parameters. In contrast, strong depth dependence of the viscosity of the folding layer limits applicability of ductile rheology and leads to a viscoelastic transition. Our theory is applied to estimate the effective thickness of the folded central Asian upper crust using the ratio of topographic wavelength to Moho depth. Phase diagrams based on geometrical parameters show that gravity does not significantly control folding in the Jura and the Zagros Mountains but does control folding in central Asia. Applicability conditions of viscous and thin sheet models for large-scale lithospheric deformation, derived in terms of the Argand number, have implications for the plate-like style of planetary tectonics. *INDEX TERMS:* 8005 Structural Geology: Folds and folding, 8020 Structural Geology: Mechanics, 8122 Tectonophysics: Dynamics, gravity and tectonics, 8149 Evolution of the Earth: Planetary tectonics (5475); *KEYWORDS:* Folding, Folds, Detachment, Décollement, Gravity, Argand

1. Introduction

[2] Folds appear on all spatial scales in nature with many forms that reflect processes involved during folding. Folding, or buckling, is a common response of layered rocks to deformation, and folds are described from the microscale (crenulation) to the regional scale [e.g., *Whitten*, 1966; *Ramsay and Huber*, 1987; *Twiss and Moores*, 1992]. Many analytical studies have investigated the mechanics of buckling, that is, layer-parallel shortening of a single, competent layer embedded in a weaker matrix [e.g., *Biot*, 1965; *Ramberg*, 1981; *Johnson and Fletcher*, 1994]. Analytical methods are mainly applied to the initial stages of folding where fold amplitudes are infinitesimal. The analytical studies differ in whether they are concerned with small-scale or large-scale folds. Small-scale studies assume that mesoscopic folds are too small to be affected by gravity and take into consideration the resistance of the matrix [e.g., *Biot*, 1961; *Currie et al.*, 1962; *Ramberg*, 1963; *Chapple*, 1968; *Fletcher*, 1974; *Smith*, 1977; *Hunt et al.*, 1996]. Large-scale studies treat structures that are large enough to respond to the effects of gravity but neglect matrix resistance (inviscid matrix), which is assumed to be small compared to resistance caused by gravitational effects [e.g., *Ramberg and Stephansson*, 1964; *Turcotte and Schubert*, 1982]. Whatever the scale, an important result of these analytical studies is a maximum of amplification rate for a certain fold wavelength, which is designated the dominant wavelength [*Biot*, 1961]. Dominant wavelengths of small-scale folds were investigated for elastic [e.g., *Biot*, 1961], elastoplastic [e.g., *Johnson*, 1980], viscous [e.g., *Biot*, 1961], ductile (non-Newtonian, power law) [e.g., *Fletcher*, 1974], and viscoelastic [e.g., *Schmalholz and Podladchikov*, 1999, 2001a] layers embedded in an infinitely thick (half-space) matrix and for elastic layers resting on a viscoelastic matrix [e.g., *Hunt et al.*, 1996], elastic layers resting on a finite, viscous matrix [*Sridhar et al.*, 2001], and viscous layers embedded in a finite, viscous matrix [*Ramberg*, 1963]. Dominant wavelengths of large-scale folds were expressed for elastic [*Ramberg and Stephansson*, 1964; *Turcotte and Schubert*, 1982] and ductile [*Burov and Molnar*, 1998; *Cloetingh et al.*, 1999] layers. In nature, both gravity and matrix resistance affect rock folding simultaneously, and several studies investigated this [e.g., *Zuber*, 1987; *Martinod and Davy*, 1992; *Goff et al.*, 1996]. However, there is no simple analytical expression for the size of folds at which there is a switch from matrix to gravity resistance as the controlling folding factor. Our first goal is to investigate the transition between matrix- and gravity-controlled folding modes and to provide a quantitative answer to the question: What does large-scale mean in the context of folding?

[3] Another shortcoming of many existing analytical theories is that the matrix is considered to be infinitely thick. This consideration allows the use of a half-space formulation for the vertical stress exerted by the matrix onto the layer boundaries. However, in many natural situations and especially in detachment folding [e.g., *Epard and Groshong*, 1995; *Poblet and McClay*, 1996] the weak matrix is thinner than the competent, folded layer. For small-scale folds (i.e., matrix-controlled), *Ramberg* [1963] showed that depending on the ratio of matrix thickness to layer thickness, a compressed layer embedded in a weaker matrix of finite thickness develops

[1]Now at Geomodelling Solutions GmbH, Zürich, Switzerland.

0148-0227/02/2001JB000355$09.00

smaller dominant wavelengths than it does in an infinitely thick matrix. The so-called thick-plate analysis is the appropriate tool to investigate both small- and large-scale detachment folding [*Goff et al.*, 1996]. Our second goal is to provide a simple analytical description of detachment folding, i.e., folding of layers resting on a matrix with finite thickness, which is more appropriate for most geological situations than the infinite half-space approximation.

[4] For these purposes, folding of a ductile (non-Newtonian, power law) layer resting on a finite, viscous matrix under the effects of gravity is studied analytically in two dimensions using linear stability analysis and thin-plate methods [e.g., *Timoshenko and Woinowsky-Krieger*, 1959; *Drazin and Reid*, 1981] (Figure 1). Our main concern in this treatment is to obtain a transparent unified analytic treatment that makes the accounting of a number of coupled processes tractable. To this end, we sacrifice precision, a decision partly justified by the uncertainty in geological parameters. Both layer and matrix are assumed to have homogeneous material properties that are independent of pressure and temperature. Natural cases are more complicated, in particular, on the lithospheric scale. However, this study does not intend to fully investigate folding lithospheric but focuses on quantifying the interaction of gravity and matrix resistance on folding characteristics.

[5] We derive critical parameters that define the transitions between matrix-controlled, gravity-controlled, and detachment folding. We introduce a single parameter S, which combines the effective viscosity contrast and the Argand number. S determines the transition from gravity-controlled to matrix-controlled folding and defines the layer thickness at which gravity becomes significant. A similar analysis is conducted for the detachment folding mode. We show that the decay of matrix viscosity with depth (due to temperature increase with depth) affects folding only for a narrow range of parameters. We also establish the range of applicability for ductile rheology as the effective rheology of competent layers on a lithospheric scale considering a depth-dependent layer viscosity and a viscoelastic rheology of the competent layer.

[6] Our final goal is to construct a phase diagram that defines the conditions for matrix-controlled, gravity-controlled, and detachment mode folding. This phase diagram is based on coordinates that depend both on material and geometrical parameters. We modify this phase diagram to be dependent on only measurable geometrical parameters by expressing poorly constrained rheological properties through an additional geometrical observable [e.g., *Schmalholz and Podladchikov*, 2001b]. Such a phase diagram is then applied to estimate the effective thickness of the folded upper crust in central Asia [e.g., *Burov et al.*, 1993], using geological information such as the ratio of topographic wavelength to detachment depth (Moho). The phase diagram is also applied to folds in the Jura and the Zagros Mountains.

2. Folding of a Ductile Layer Resting on an Infinite, Viscous Matrix Affected by Gravity

[7] We use linear stability analysis [e.g., *Drazin and Reid*, 1981] to investigate an axially compressed, ductile layer resting horizontally on an infinite, viscous matrix in two dimensions. Assuming vertical gravity and neglecting the shear stresses exerted by the matrix onto the layer boundary, the thin-plate theory provides a single equilibrium equation for the folded layer [e.g., *Timoshenko and Woinowsky-Krieger*, 1959; *Reddy*, 1999]:

$$\frac{\partial^2}{\partial x^2}\left(\int_{-H/2}^{H/2} z\sigma_{xx}dz\right)+\frac{\partial}{\partial x}\left(\int_{-H/2}^{H/2}\frac{\partial W(x,t)}{\partial x}\sigma_{xx}dz\right)$$

$$+q_m-\Delta\rho g W(x,t)=0, \qquad (1)$$

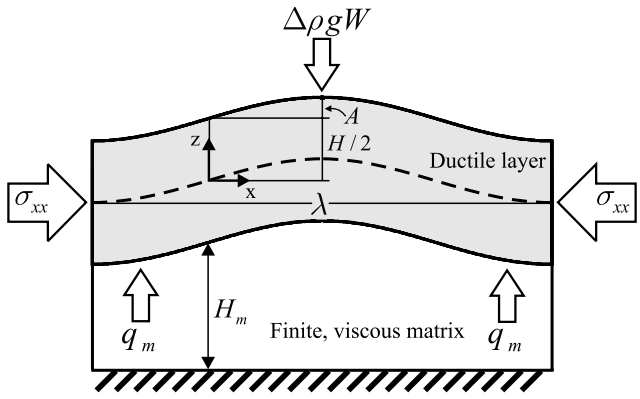

Figure 1. Schematic model of folding of a ductile single-layer resting on a finite, viscous matrix affected by gravity. $\Delta\rho gW$ is the stress caused by gravity, σ_{xx} is the compressive stress, q_m is the vertical stress caused by the resistance of the matrix, H is the layer thickness, H_m is the thickness of the matrix, A is the amplitude, and λ is the wavelength.

where x and z are horizontal and vertical coordinates, respectively, H is the thickness of the layer, $W(x,t)$ is the deflection of the layer, t is the time, $\Delta\rho$ is the density difference between the material below and above the layer, g is the gravity acceleration, σ_{xx} is the layer-parallel stress, and q_m is the vertical component of the stress exerted by the matrix onto the layer boundary (Figure 1).

[8] For a ductile material the horizontal deviatoric stress τ_{xx} can be approximated as [*England and McKenzie*, 1982]

$$|\tau_{xx}| = B|\dot{\varepsilon}_{xx}|^{\frac{1}{n}}, \qquad (2)$$

where $\dot{\varepsilon}_{xx}$ is the strain rate in the x direction, B is a material constant (averaged across the layer), and n is the power law exponent. The strain rate can be split into a mean (averaged over layer thickness) and a fiber component [e.g., *Timoshenko and Woinowsky-Krieger*, 1959; *Reddy*, 1999]:

$$\dot{\varepsilon}_{xx} = -\dot{\varepsilon}_B + \dot{\varepsilon}_F, \qquad (3)$$

where $\dot{\varepsilon}_B$ is the absolute value of the mean layer-parallel strain rate caused by shortening and $\dot{\varepsilon}_F$ is the fiber strain rate caused by flexure, or bending, of the layer [cf. *Schmalholz and Podladchikov*, 2000]. Substituting (3) into (2) and expanding the nonlinear equation (2) by a Taylor series around $\dot{\varepsilon}_F = 0$ (i.e., not bended layer) provides a linear approximation for the deviatoric stress [e.g., *Fletcher and Hallet*, 1983]:

$$\tau_{xx} = -2\mu_{\text{eff}}\dot{\varepsilon}_B + 2\frac{\mu_{\text{eff}}}{n}\dot{\varepsilon}_F, \qquad (4)$$

where μ_{eff} is the effective viscosity of the layer given by

$$\mu_{\text{eff}} = \frac{B}{2}\dot{\varepsilon}_B^{\left(\frac{1}{n}-1\right)}. \qquad (5)$$

Note that $B = 2\mu_l$ if $n = 1$ with μ_l being the viscosity of the layer. An expression for the total layer-parallel stress σ_{xx} can be found by assuming that $\sigma_{zz} = 0$ throughout the layer (i.e., constant thickness). Then, for incompressible materials (i.e., $\dot{\varepsilon}_{xx} = -\dot{\varepsilon}_{zz}$) the total layer-parallel stress is twice the deviatoric stress in the x direction [*Turcotte and Schubert*, 1982]:

$$\sigma_{xx} = -P + 4\frac{\mu_{\text{eff}}}{n}\dot{\varepsilon}_F, \qquad (6)$$

where

$$P = 4\mu_{\text{eff}}\dot{\varepsilon}_B \tag{7}$$

is the mean (averaged over layer thickness) layer-parallel stress. Assuming no shear stresses within the ductile layer, $\dot{\varepsilon}_F$ can be expressed as [e.g., *Timoshenko and Woinowsky-Krieger*, 1959; *Turcotte and Schubert*, 1982]

$$\dot{\varepsilon}_F = -z\frac{\partial^3 W(x,t)}{\partial x^2 \partial t} \tag{8}$$

The vertical stress of an infinitely thick matrix (half-space) that acts on one layer boundary is given by [*Biot*, 1961]

$$q_m = -2\mu_m \omega \frac{\partial W(x,t)}{\partial t}, \tag{9}$$

where μ_m is the viscosity of the matrix, $\omega = 2\pi/\lambda$, and λ is the wavelength of the layer perturbation. Assuming a constant layer thickness and substituting (6), (8), and (9) into (1) yields

$$\frac{\mu_{\text{eff}} H^3}{3n}\frac{\partial^5 W(x,t)}{\partial x^4 \partial t} + P H \frac{\partial^2 W(x,t)}{\partial x^2} + 2\mu_m \omega \frac{\partial W(x,t)}{\partial t} + \Delta\rho g W(x,t) = 0. \tag{10}$$

A general solution of (10) for a single waveform is of the form

$$W(x,t) = A_0 \exp(I\omega x + \alpha t), \tag{11}$$

where A_0 is the initial amplitude, α is the amplification rate of the considered layer perturbation, and $I = \sqrt{-1}$. Substituting (11) into (10), collecting the coefficients in front of $\exp(I\omega x + \alpha t)$ and solving for the amplification rate α yields [cf. *Zuber*, 1987]

$$\alpha/\dot{\varepsilon}_B = \frac{6n(2\bar{\omega}^2 - Ar)}{\bar{\omega}[\bar{\omega}^3 + 6n\mu_m/\mu_{\text{eff}}]} \tag{12}$$

where $\bar{\omega} = \omega H$ and

$$Ar = \frac{\Delta\rho g H}{2\mu_{\text{eff}}\dot{\varepsilon}_B} = \frac{\Delta\rho g H}{B\dot{\varepsilon}_B^{1/n}} \tag{13}$$

is the Argand number [e.g., *England and McKenzie*, 1982]. Equation (12) presents the amplification rate (normalized by $\dot{\varepsilon}_B$) for harmonic folding of a ductile layer resting on an infinite, viscous matrix under the effects of gravity. More generally, folding of a layer with arbitrary initial geometry (including localized perturbations) can be Fourier-analyzed into periodic contributions of different wavelengths evolving in time according to (11) and (12) and can be reconstructed by superposition of the modified components due to linearity of (10). To reduce the number of controlling parameters in (12), we introduce the following nondimensional parameters:

$$\hat{\omega} = \frac{\omega H}{\sqrt{Ar}} = \frac{2\pi H}{\lambda\sqrt{Ar}} \qquad S = \frac{9\sqrt{6}}{4}\frac{\mu_m n}{\mu_{\text{eff}} Ar^{\frac{3}{2}}}. \tag{14}$$

Note that parameters with a ''hat'' (e.g., $\hat{\omega}$) are dimensionless and scaled by other dimensionless numbers.

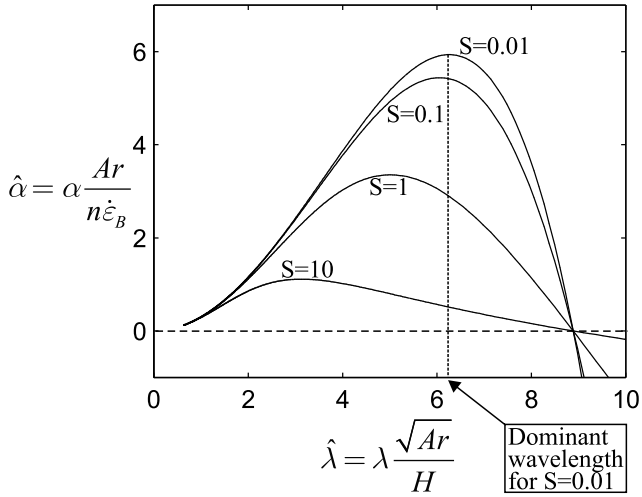

Figure 2. Dimensionless amplification rate $\hat{\alpha}$ versus fold wavelength $\hat{\lambda} = 2\pi/\hat{\omega}$. The amplification rate spectrum depends only on S (see (14) and (15)) and yields a maximal amplification rate that corresponds to a certain wavelength, which is designated the dominant wavelength.

Substituting (14) into (12) provides a dimensionless amplification rate:

$$\hat{\alpha} = \alpha\frac{Ar}{n\dot{\varepsilon}_B} = 54\frac{2\hat{\omega}^2 - 1}{\hat{\omega}\left(9\hat{\omega}^3 + 4\sqrt{6}S\right)}. \tag{15}$$

This amplification rate yields a maximum for a certain value of $\hat{\omega}$ depending solely on the parameter S (Figure 2). The maximal value of the amplification rate corresponds to the fastest growing wavelength, which is the dominant wavelength λ_{tot}. No simple explicit analytical expression for λ_{tot} from (15) could be found because the solution requires finding the roots of a polynomial of order 5. However, an explicit relationship for the S versus the dominant wave number (termed $\hat{\omega}_{\text{tot}}$) is derived by setting derivative of $\hat{\alpha}$ versus $\hat{\omega}$ to zero and solving for S:

$$S = \frac{3\sqrt{6}}{2}\frac{\hat{w}_{\text{tot}}^3\left(\hat{w}_{\text{tot}}^2 - 1\right)}{2\hat{w}_{\text{tot}}^2 + 1}. \tag{16}$$

Simple dominant wavelength expressions can be derived for the end-member situations, at which either gravity is neglected ($g = 0$ in (1), i.e., matrix-controlled) or the matrix is inviscid ($q_m = 0$ in (1), i.e., gravity-controlled) during folding. The dominant wavelength for matrix-controlled folding is [e.g., *Fletcher*, 1974]

$$\lambda_{\text{mat}} = 2\pi H\left(\frac{\mu_{\text{eff}}}{3n\mu_m}\right)^{\frac{1}{3}} \tag{17a}$$

or

$$\lambda_{\text{mat}}\frac{\sqrt{Ar}}{H} = \frac{\sqrt{6}\pi}{S^{\frac{1}{3}}}. \tag{17b}$$

The dominant wavelength for gravity-controlled folding, derived by setting $S = 0$ in (16), is

$$\lambda_{\text{grav}} = \frac{2\pi H}{\sqrt{Ar}} \tag{18a}$$

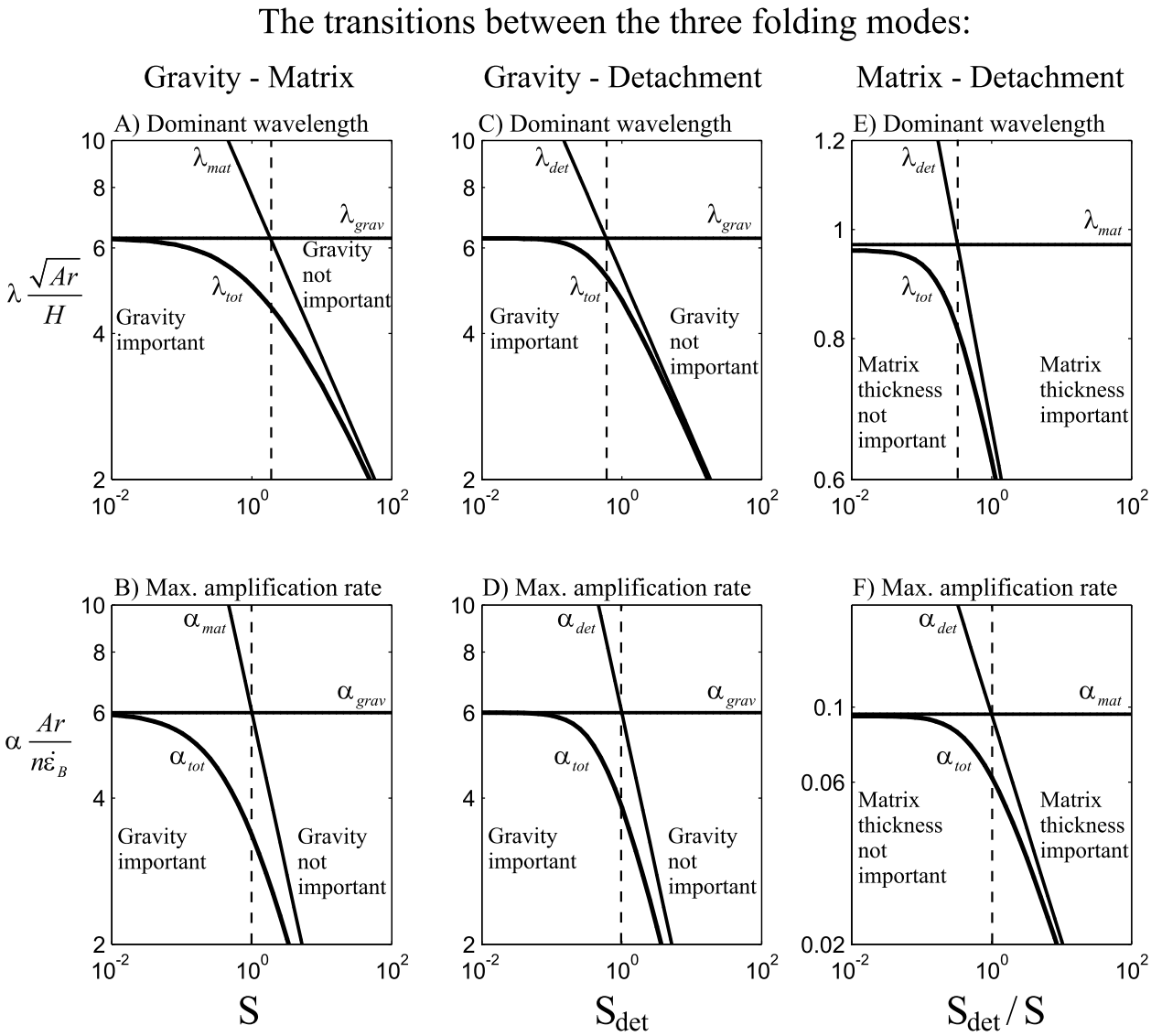

Figure 3. Dominant wavelengths and maximal amplification rates versus the controlling parameters S, S_{det}, and S_{det}/S (see text for definitions; double logarithmic scale). Every transition is controlled by only one of the controlling parameters. For each transition the corresponding two limit solutions are plotted together with the total or complete solution versus the corresponding parameter that controls the transition. The subscripts grav, mat, and det indicate the limits gravity-controlled folding, matrix-controlled folding, and detachment folding, respectively, and subscript tot indicates the complete folding solution (see text for definitions). The transitions occur when the limit solutions are equal to each other. If the controlling parameters S, S_{det}, and S_{det}/S are either much smaller or larger than one, the total solution is the same as one of the limit solutions.

or

$$\lambda_{\mathrm{grav}}\frac{\sqrt{Ar}}{H}=2\pi. \tag{18b}$$

The dominant wavelengths λ_{mat} and λ_{grav} are plotted together with λ_{tot} versus the parameter S in Figure 3a. The maximal values of the amplification rates are obtained by back substitution of the dominant wavelengths (17) and (18) to the amplification rate (15). The maximal amplification rate for matrix-controlled folding is

$$\alpha_{\mathrm{mat}}=4n^{\frac{1}{3}}\left(\frac{\mu_{\mathrm{eff}}}{3\mu_m}\right)^{\frac{2}{3}}\dot{\varepsilon}_B \tag{19a}$$

or

$$\alpha_{\mathrm{mat}}\frac{Ar}{n\dot{\varepsilon}_B}=\frac{6}{S^{\frac{2}{3}}}. \tag{19b}$$

The maximal amplification rate for gravity-controlled folding is

$$\alpha_{\mathrm{grav}}=\frac{6n}{Ar}\dot{\varepsilon}_B \tag{20a}$$

or

$$\alpha_{\mathrm{grav}}\frac{Ar}{n\dot{\varepsilon}_B}=6. \tag{20b}$$

An expression for the maximal amplification rate of the complete (15) (termed α_{tot}) is obtained by eliminating S in (15) using (16):

$$\hat{\alpha}_{\mathrm{tot}}=2\frac{2\hat{w}_{\mathrm{tot}}^2+1}{\hat{w}_{\mathrm{tot}}^4}. \tag{21}$$

Table 1. Conditions and Results for the Three Modes of Folding[a]

Folding Mode	Formal Conditions	Spelled Out Conditions	Dominant Wavelength	Maximum Amplification Rate
Gravity-controlled	$\alpha_{grav} < \alpha_{mat}$ $\alpha_{grav} < \alpha_{det}$	$H > 3\left(\frac{3n\mu_m}{\mu_{eff}}\right)^{\frac{2}{3}}\frac{\mu_{eff}\dot{\varepsilon}_B}{\Delta\rho g}$ $H_m > 4\left(\frac{3n\mu_m}{\mu_{eff}}\right)^{13}\frac{\mu_{eff}\dot{\varepsilon}_B}{\Delta\rho g}$	$\frac{2\pi}{\sqrt{Ar}}H$	$\frac{6n}{Ar}\dot{\varepsilon}_B$
Matrix-controlled	$\alpha_{mat} < \alpha_{grav}$ $\alpha_{mat} < \alpha_{det}$	$H < 3\left(\frac{3n\mu_m}{\mu_{eff}}\right)^{\frac{2}{3}}\frac{\mu_{eff}\dot{\varepsilon}_B}{\Delta\rho g}$ $H_m > \frac{4}{3}\left(\frac{\mu_{eff}}{3nm_m}\right)^{\frac{1}{3}}H$	$2\pi\left(\frac{\mu_{eff}}{3n\mu_m}\right)^{\frac{1}{3}}H$	$4n\left(\frac{\mu_{eff}}{3n\mu_m}\right)^{\frac{2}{3}}\dot{\varepsilon}_B$
Detachment	$\alpha_{det} < \alpha_{grav}$ $\alpha_{det} < \alpha_{mat}$	$H_m < 4\left(\frac{3n\mu_m}{\mu_{eff}}\right)^{\frac{1}{3}}\frac{\mu_{eff}\dot{\varepsilon}_B}{\Delta\rho g}$ $H_m < \frac{4}{3}\left(\frac{\mu_{eff}}{3n\mu_m}\right)^{\frac{1}{3}}H$	$1.2\pi\left(\frac{\mu_{eff}}{3n\mu_m}\right)^{\frac{1}{6}}\sqrt{\frac{H_m}{H}}H$	$3n\left(\frac{\mu_{eff}}{3n\mu_m}\right)^{\frac{1}{3}}\frac{H_m}{H}\dot{\varepsilon}_B$

[a] The maximal amplification rate that controls the folding mode is the minimum out of the three maximal amplification rates corresponding to matrix-controlled, gravity-controlled, and detachment folding (i.e., $\alpha_d = \min(\alpha_{grav}, \alpha_{mat}, \alpha_{det})$). The slowest of the three amplification rates represents the strongest resistance against folding (i.e., either due to gravity, matrix viscosity, or matrix thickness) and therefore controls the fold amplification. Note that for all folding modes, there is the same approximate relationship between the maximal amplification rate and the dominant wavelength, specifically $\alpha_d/\dot{\varepsilon}_B \approx (\lambda_d/H)^2 n/\pi^2$.

The amplification rates α_{mat} and α_{grav} are plotted versus S in Figure 3b together with α_{tot} plotted parametrically using (16) and (21). If S goes to zero, α_{tot} approaches asymptotically α_{grav} (the gravity-controlled limit). If, instead, S goes to infinity, α_{tot} approaches asymptotically α_{mat} (the matrix-controlled limit, Figure 3b). The ratio

$$\frac{\alpha_{grav}}{\alpha_{mat}} = S^{\frac{2}{3}} \tag{22}$$

is equal to one if α_{grav} and α_{mat} are identical (Figure 3b). During folding, the two simultaneous resistances caused by gravity and matrix viscosity interact in parallel, i.e., the total resistance controlled by the strongest resistance. The strongest resistance corresponds to the smallest (or slowest) amplification rate. Therefore, if $S < 1$, then $\alpha_{grav} < \alpha_{mat}$ and the folding is by the slower gravity-controlled mode; otherwise, $\alpha_{mat} < \alpha_{grav}$ and matrix viscosity dominates resistance to folding. Similar results were obtained by *Schmalholz and Podladchikov* [2001a] for a viscoelastic layer with Kelvin rheology (parallel combination of elastic and viscous elements), where the strongest resistance controls folding. In contrast, for folding of a viscoelastic layer with Maxwell rheology (serial combination of elastic and viscous elements) the weakest resistance controls folding [cf. *Schmalholz and Podladchikov*, 2001a].

3. Folding of a Ductile Layer Resting on a Finite, Viscous Matrix Affected by Gravity

[9] We consider the same setting as above (Figure 1), but because the matrix now has finite thickness, a new expression for the vertical stress, q_m (equation (9)), that the viscous matrix exerts on the layer is necessary. Assuming an incompressible viscous matrix the equation of continuity is given by

$$\frac{\partial v_x}{\partial x} + \frac{\partial v_z}{\partial z} = 0, \tag{23}$$

where v_x and v_z are the velocities in the x and z directions, respectively. Equation (23) is used to express v_x through v_z. We split the velocity into a background component due to shortening and a perturbed component due to folding [e.g., *Johnson and Fletcher*, 1994]:

$$\begin{aligned} v_z &= \tilde{v}_z(z)\exp(I\omega x) + \dot{\varepsilon}_B z \\ v_x &= \tilde{v}_x(z)\exp(I\omega x) - \dot{\varepsilon}_B x \end{aligned} \tag{24}$$

where $\tilde{v}_z(z)$ and $\tilde{v}_x(z)$ are velocity coefficients dependent only on z. The equations of equilibrium for slow viscous flow in two dimensions are given by [e.g., *Mase*, 1970]

$$\frac{\partial \sigma_{xx}}{\partial x} + \frac{\partial \tau_{xz}}{\partial z} = 0 \tag{25}$$

$$\frac{\partial \tau_{xz}}{\partial x} + \frac{\partial \sigma_{zz}}{\partial z} = 0, \tag{26}$$

where τ_{xz} is the shear stress and σ_{zz} is the vertical normal stress. The stresses are given by Newtonian viscous rheology:

$$\begin{aligned} &\sigma_{xx} = -p + 2\mu_m\frac{\partial v_x}{\partial x}, \qquad \sigma_{zz} = -p + 2\mu_m\frac{\partial v_z}{\partial z}, \\ &\tau_{xz} = \mu_m\left(\frac{\partial v_x}{\partial z} + \frac{\partial v_z}{\partial x}\right), \end{aligned} \tag{27}$$

where p is the pressure. Substituting the velocities expressions (24) into (27) and stress expressions (27) into (25) and (26), taking the partial derivative of (25) with respect to z and subtracting from it the partial derivative of (26) with respect to x, using (23) and (24) to eliminate $\tilde{v}_x(z)$, and collecting coefficients in front of $\exp(I\omega x)$ yields [e.g., *Johnson and Fletcher*, 1994]

$$\frac{\partial^4 \tilde{v}_z(z)}{\partial z^4} - 2\omega^2\frac{\partial^2 \tilde{v}_z(z)}{\partial z^2} + \omega^4\tilde{v}_z(z) = 0 \tag{28}$$

Four boundary conditions are required to solve (28), which we set as

$$\begin{aligned} &\tilde{v}_z(0) = \tfrac{\partial W(x,t)}{\partial t}, \qquad \tfrac{\partial \tilde{v}_z(0)}{\partial z} = 0, \\ &\tilde{v}_z(H_m) = 0, \qquad \tfrac{\partial \tilde{v}_z(H_m)}{\partial z} = 0, \end{aligned} \tag{29}$$

where H_m is the thickness of the viscous matrix (Figure 1). The physical meaning of the boundary conditions is that there is no slip between the matrix and the layer (i.e., bonded contact) and the matrix and the rigid bottom (note that $\partial \tilde{v}_z/\partial z = 0 \Rightarrow \tilde{v}_x = 0$, compare (23) and (24)). Equation (28) is solved for $\tilde{v}_z(z)$; this permits calculation of v_z and v_x using (23) and (24). Next, τ_{xz} and p are calculated using (27) and (26), respectively. Finally, the vertical stress of the finite, viscous matrix q_m is calculated using (27):

$$q_m = \sigma_{zz} = -2\mu_m\omega\frac{\partial W(x,t)}{\partial t}F_{det}. \tag{30}$$

Equation (30) is similar to that for an infinitely thick matrix (compare (9)) but multiplied by a function F_{det} that depends only on the dimensionless product of ω and H_m and is given by

$$F_{det} = \frac{-1 + 4\omega H_m\exp(2\omega H_m) + \exp(4\omega H_m)}{1 - \left(2 + 4\omega^2 H_m^2\right)\exp(2\omega H_m) + \exp(4\omega H_m).} \tag{31}$$

$F_{det} \to 1$ when $\omega H_m \to \infty$, and $F_{det} \approx 6/(\omega H_m)^3$ when $\omega H_m \to 0$.

Therefore the stress expression in (30) approaches the half-space stress expression presented in (9) with increasing H_m. A similar result for the vertical stress exerted by a finite, viscous matrix on the layer boundary was recently presented by *Sridhar et al.* [2001] but for free slip conditions ($\tau_{xz} = 0$ at layer-matrix boundary). *Sridhar et al.* [2001] investigated buckling of an elastic layer resting on a finite, viscous matrix without the effects of gravity. Equations (30) and (31) are substituted into (1), and the resulting nondimensional amplification rate for folding of a ductile layer resting on a finite, viscous matrix under the effects of gravity is

$$\alpha/\dot{\varepsilon}_B = \frac{6n\left(2\bar{\omega}^2 - Ar\right)}{\bar{\omega}\left(\bar{\omega}^3 + 6nF_{\text{det}}\mu_m/\mu_{\text{eff}}\right)}. \tag{32}$$

Using the approximation $F_{\text{det}} \approx 1 + 6/(\omega H_m)^3$, which is valid with the good accuracy over the entire parameter range, this amplification rate can be alternatively expressed through the parameters $\hat{\omega}$, S, and S_{det}, yielding (compare (15))

$$\hat{\alpha} = \alpha\frac{Ar}{n\dot{\varepsilon}_B} = 54\frac{2\hat{\omega}^2 - 1}{\hat{\omega}\left(9\hat{\omega}^3 + 4\sqrt{6}S + 13.5S_{\text{det}}^2/\hat{\omega}^3\right)}, \tag{33}$$

where

$$S_{\text{det}} = \sqrt{\frac{24n\mu_m/\mu_{\text{eff}}}{\left(ArH_m/H\right)^3}} \tag{34}$$

and $\hat{\alpha}$ has a single maximum for a function of $\hat{\omega}$ depending on both S and S_{det}.

[10] If the matrix thickness H_m decreases below a critical value, then folding is strongly controlled by the ratio H_m/H. We designate this additional folding mode as detachment folding. Approximate expressions of the dominant wavelength and maximal amplification rates for detachment folding are found using Taylor expansions for $H_m/H \rightarrow 0$. For detachment folding, the dominant wavelength is given by

$$\lambda_{\text{det}} = 1.2\pi\left(\frac{\mu_{\text{eff}}}{3n\mu_m}\right)^{\frac{1}{6}}\sqrt{\frac{H_m}{H}}H \tag{35a}$$

or

$$\lambda_{\text{det}}\frac{\sqrt{Ar}}{H} = \frac{2\pi}{\left(5S_{\text{det}}/3\right)^{\frac{1}{3}}}, \tag{35b}$$

and the maximal amplification rate is

$$\alpha_{\text{det}} = 3n\left(\frac{\mu_{\text{eff}}}{3n\mu_m}\right)^{\frac{1}{3}}\frac{H_m}{H}\dot{\varepsilon}_B \tag{36a}$$

or

$$\alpha_{\text{det}}\frac{Ar}{n\dot{\varepsilon}_B} = \frac{6}{S_{\text{det}}^{\frac{2}{3}}}. \tag{36b}$$

[11] The folding solution presented in (33) quantifies the entire set of folding modes (matrix-controlled, gravity-controlled, and detachment folding) and their mutual transitions. In section 2 the transition between matrix-controlled and gravity-controlled folding ($S_{\text{det}} = 0$ in (33)) was investigated (Figure 3a and 3b). The solutions for detachment folding (equations (35) and (36)) allow us to investigate the transitions between gravity-controlled and detachment folding (Figures 3c and 3d) and between matrix-controlled and detachment folding (Figures 3e and 3f). Since gravity is only important if $S < 1$, setting $S = 0$ allows us to investigate the transition between the gravity-controlled and the detachment folding mode as a function of the single parameter S_{det} (Figures 3c and 3d). Alternatively, if $S \gg 1$, then gravity is unimportant and setting S to a large number (e.g., 500) causes the transition between the matrix-controlled and the detachment folding mode to be a function of the single parameter S_{det}/S (Figures 3e and 3f). The parameters S and S_{det} were defined in such a way that all three transitions for the maximal amplification rates occur when the controlling parameters S, S_{det}, and S_{det}/S have values of unity. The conditions for the three transitions and the solutions for each folding mode are listed in Table 1.

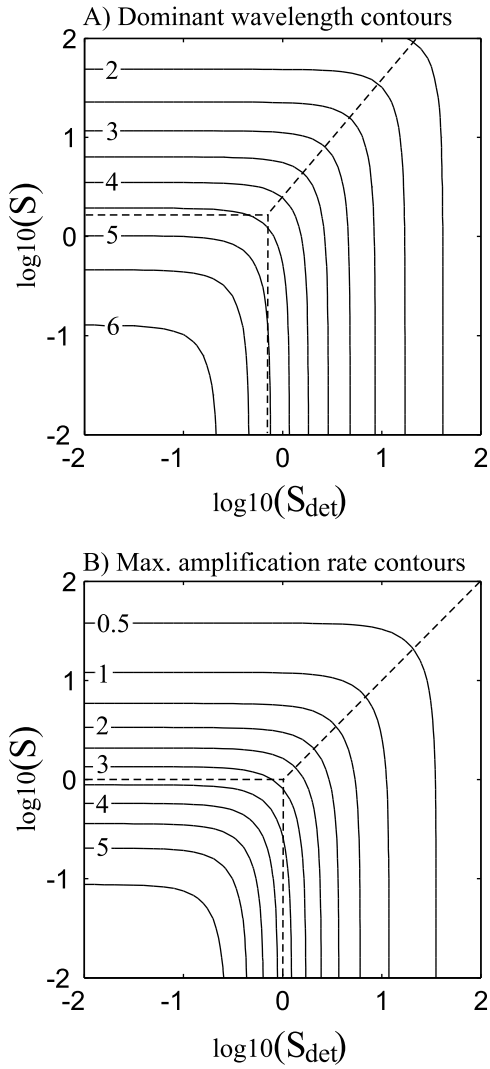

Figure 4. Contours of the dominant wavelength and the maximal amplification rate in the space $S - S_{\text{det}}$. (a) The dashed lines indicate the three transitions shown in Figures 3a, 3c, and 3e. (b) The transitions between the three folding modes (gravity-controlled, matrix-controlled, and detachment folding) occur at the dashed lines $S = 1$, $S_{\text{det}} = 1$, and $S = S_{\text{det}}$ (see Figures 3b, 3d, and 3f). These lines separate areas with three different contour patterns: (1) only horizontal contours corresponding to matrix-controlled folding, (2) only vertical contours corresponding to detachment folding, and (3) curved contours corresponding to gravity-controlled folding (see also Figure 5).

[12] The dominant wavelengths and the corresponding maximal amplification rates derived from the general amplification rate (equation (33)) are contoured in the $S - S_{\text{det}}$ space (Figure 4). Considering the maximal amplification rates (Figures 3b, 3d, and 3f), the three transitions occur at the lines $S = 1$, $S_{\text{det}} = 1$, and $S_{\text{det}} = S$. In the space $S - S_{\text{det}}$ these lines separate three areas with different contour patterns (Figure 4b): horizontal contours corresponding to matrix-controlled folding, vertical contours corresponding to detachment folding, and curved contours corresponding to gravity-controlled folding. Noting that $S = (\alpha_{\text{grav}}/\alpha_{\text{mat}})^{3/2}$ and $S_{\text{det}} =$

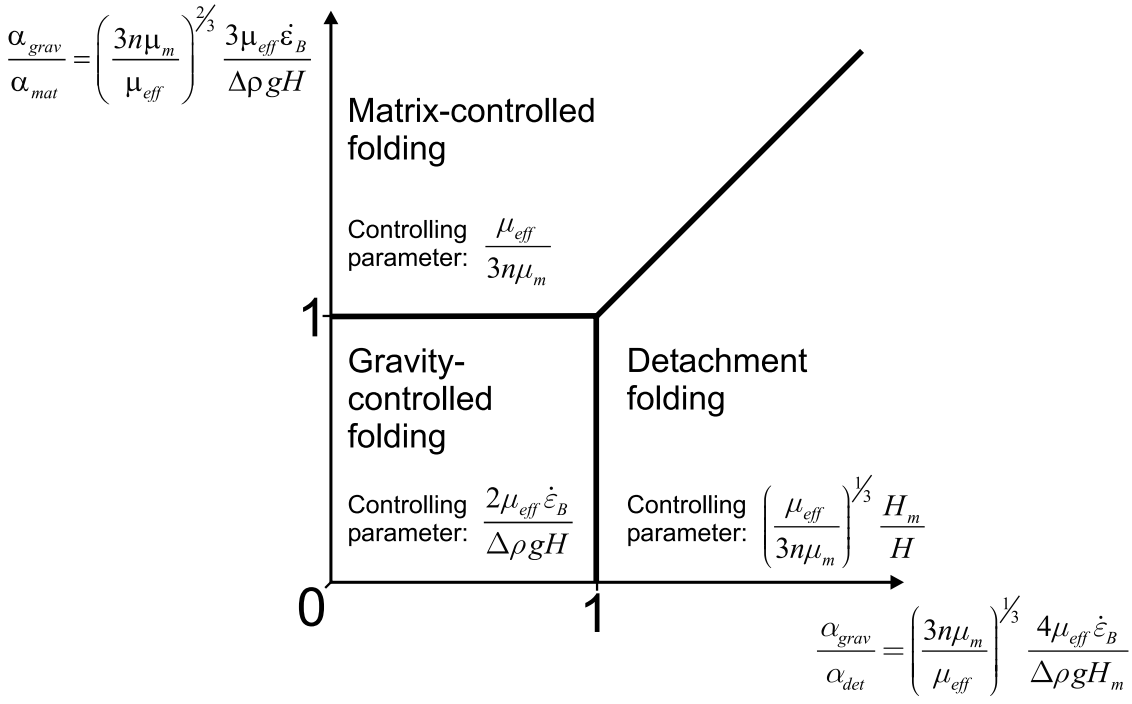

Figure 5. The phase diagram for folding distinguishes three folding modes using the two dimensionless ratios $\alpha_{grav}/\alpha_{mat}$ and $\alpha_{grav}/\alpha_{det}$. Every folding mode depends on one parameter which controls both the dominant wavelength and the maximal amplification rate (see also Table 1).

$(\alpha_{grav}/\alpha_{det})^{3/2}$, we can construct a phase diagram in the space $\alpha_{grav}/\alpha_{mat}$ – $\alpha_{grav}/\alpha_{det}$ (Figure 5). Of the three end-member folding modes the active folding mode is the one with the smallest amplification rate.

[13] For detachment folding, decreasing the matrix thickness H_m causes a decrease in the dominant wavelength and the maximal amplification rate. Results obtained with our analytical theory compare well with analytical and analogue results obtained by *Ramberg* [1963] for folding, while the matrix above and below the layer has the same finite thickness and gravity can be ignored. *Sridhar et al.* [2001] showed that for folding of an elastic layer resting on a finite, viscous matrix, both the dominant wavelength and the maximal amplification rate decrease with decreasing matrix thickness. Therefore the matrix thickness has the same influence on the dominant wavelength and the maximal amplification rate, independent of layer rheology for both free slip and no slip between layer and matrix.

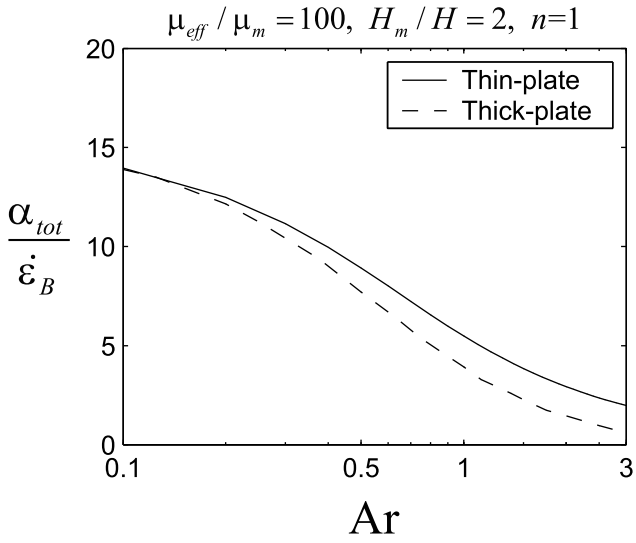

Figure 6. Comparison of the thin-plate and thick-plate solutions. The maximal amplification rate ($\alpha_{tot}/\dot{\varepsilon}_B$, corresponding to the dominant wavelength) is plotted versus the Argand number (Ar). For $Ar > \approx 0.2$ the thin-plate results start to deviate from the thick-plate results. The comparison is done for a matrix thickness (H_m) twice thicker than the layer thickness (H), a viscosity contrast (μ_{eff}/μ_m) of 100 and a power law exponent (n) of 1.

[14] To verify our analytical approximations, we derived a more accurate solution for folding of a ductile layer resting on a finite, viscous matrix affected by gravity using the perturbation or "thick-plate" method. The perturbation method is a standard method to investigate instability problems [e.g., *Lin and Segel*, 1974; *Drazin and Reid*, 1981] and is frequently applied to instability problems in geodynamics [e.g., *Smith*, 1977; *Fletcher and Hallet*, 1983; *Ricard and Froidevaux*, 1986; *Zuber*, 1987; *Bassi and Bonnin*, 1988; *Goff et al.*, 1996]. The results provided by the perturbation method are in good agreement with our results derived using thin-plate assumptions (Figure 6). The strongest discrepancy between the methods is observed for maximal amplification rates at high Argand number (i.e., $Ar > \approx 2$). For example, for a Newtonian viscous layer and $H_m/H >> 1$ the thin-plate method yields a maximal amplification rate smaller than one (i.e., $\alpha_{tot}/\dot{\varepsilon}_B < 1$) for $Ar > 6$ (compare (20)), whereas the perturbation method provides values of $\alpha_{tot}/\dot{\varepsilon}_B < 1$ for $Ar > \approx 2.5$.

4. Folding of a Ductile Layer Resting on a Matrix With Depth-Dependent Viscosity

[15] In nature, the viscosities of the layer and the matrix are strongly dependent on depth due to temperature variations [e.g., *Braun and Beaumont*, 1987], especially on the crustal and lithospheric scales. On such scales the depth extent of the matrix rocks involved in folding deformation is generally greater than the thickness of the competent layer, and therefore the depth depend-

ence of the matrix viscosity must be considered first. The matrix viscosity is approximately an exponential function of depth [e.g., *Fletcher and Hallet*, 1983; *Zuber*, 1987; *Shen et al.*, 2001]

$$\mu_M(z) = \mu_m \exp(z/\zeta), \tag{37}$$

where μ_m is the viscosity of the matrix at the layer-matrix boundary and ζ is the *e*-fold length of the viscosity variation (Figure 7). Using the same approach as in section 3, we can derive an expression for the vertical stress q_m exerted on the competent layer by an infinitely thick matrix with exponentially varying viscosity. The vertical stress is given by

$$q_m = -2\mu_m \omega \frac{\partial W(x,t)}{\partial t} F_{dd}, \tag{38}$$

where

$$F_{dd} = \frac{\left(2 - \sqrt{2Z + 2 + 8(\omega\zeta)^2}\right)(Z+1) + 16(\omega\zeta)^2}{16(\omega\zeta)^3}, \tag{39}$$

with $Z = \sqrt{1 + 24(\omega\zeta)^2 + 16(\omega\zeta)^4}$. F_{dd} depends only on the dimensionless product of ω and ζ. $F_{dd} \to 1$ when $\omega\zeta \to \infty$, and $F_{dd} \to 4(\omega\zeta)^3$ when $\omega\zeta \to 0$. Therefore the stress expression in (38) approaches the half-space stress expression presented in (9) for increasing ζ. Substituting (38) and (39) into (1) yields the amplification rate (compare (32)):

$$\alpha\dot{\varepsilon}_B = \frac{6n(2\bar{\omega}^2 - Ar)}{\bar{\omega}(\bar{\omega}^3 + 6nF_{dd}\mu_m/\mu_{\text{eff}})}. \tag{40}$$

If $Ar = 0$, this amplification rate yields a maximum for a specific dominant wavelength only for values of H/ζ smaller than some critical value (see below). Folding of a layer resting on a matrix with depth-dependent viscosity can be described by the results for matrix-controlled folding if an enlarged (effective) layer thickness is introduced. A close approximation for the dominant wavelength, λ_{dd}, is then

$$\lambda_{dd} \approx \lambda_{\text{mat}} \Big/ \left(1 - \frac{4}{5}E\right) \tag{41}$$

with

$$E = \left(\frac{\mu_{\text{eff}}}{n\mu_m}\right)^{\frac{1}{3}} \frac{H}{\zeta}.$$

The critical parameter that determines the deviation from λ_{mat} is E, which depends on the viscosity contrast at the layer-matrix boundary and the ratio of the layer thickness to the *e*-fold length of the viscosity variation. If E is much smaller than one, then $\lambda_{dd} \approx \lambda_{\text{mat}}$. If E is $\sim$1/2, then λ_{dd} is $\sim$65% larger than λ_{mat}, and if E approaches 5/4, then λ_{dd} goes to infinity, which corresponds to matrix-controlled folding with an infinitely large viscosity contrast.

[16] As for the other folding modes (see Table 1), the dependence of the maximal amplification rate on the dominant wavelength follows the same general relation given by

$$\frac{\alpha_{dd}}{\dot{\varepsilon}_B} \approx \frac{n}{\pi^2}\left(\frac{\lambda_{dd}}{H}\right)^2 \tag{42}$$

Equations (41) and (42) show that $\alpha_{dd} \to \infty$ when $E \to 5/4$, which arguably would replace this folding mode with another mode, such as gravity-controlled or detachment folding, with finite growth rate. Indeed, restoring the gravity term ($Ar \neq 0$) in (40) and using the approximation $F_{dd} \to 4(\omega\zeta)^3$ valid for $\omega\zeta \to 0$ (or $E > 1$) yields

$$\alpha/\dot{\varepsilon}_B = \frac{6n(2\bar{\omega}^2 - Ar)}{(1 + 24n/E^3)\bar{\omega}^4}. \tag{43}$$

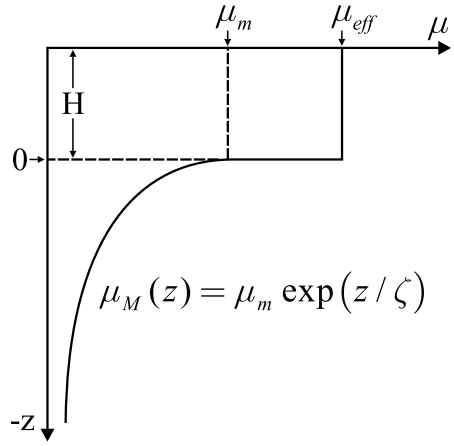

Figure 7. Viscosity profile for folding of a ductile layer resting on an infinitely thick matrix with depth-dependent viscosity. The viscosity of the matrix decreases exponentially with depth controlled by the *e*-fold length ζ. There is a viscosity step at the boundary between layer and matrix from μ_{eff} to μ_m, respectively.

The expression for the dominant wavelength is identical to the gravity-controlled limit (compare (18)):

$$\lambda_{dd} = \lambda_{\text{grav}} = \frac{2\pi H}{\sqrt{Ar}}. \tag{44}$$

The maximal amplification rate in this limit is

$$\alpha_{dd} = \frac{6n\dot{\varepsilon}_B}{(1 + 24n/E^3)Ar} = \frac{\alpha_{\text{grav}}}{1 + 24n/E^3}, \tag{45}$$

which can be reduced to the gravity limit by introducing an effective power low exponent:

$$n_{\text{eff}} = \frac{n}{1 + 24n/E^3}. \tag{46}$$

This definition slightly widens the gravity-controlled folding field on the phase diagram (Figure 5) due to the depth dependence of the matrix viscosity. However, the general recipe for determining the folding mode remains the same; that is, there is no need to introduce an additional folding mode. We conclude that the folding mode considered in this section has a limited range of applicability, i.e., for $0.1 < E < 1.25$ (if $E < 0.1$, then $\lambda_{dd} \approx \lambda_{\text{mat}}$; if $E > 1.25$, then $\lambda_{dd} \approx \lambda_{\text{grav}}$). Interestingly, through replacing H by ζ, the thin-plate results (equations (44) and (45)) represent the true long-wavelength (or $Ar < 0.1$) limit for folding of a viscous half-space with exponentially decreasing viscosity in the gravity field [cf. *Biot*, 1961, equations (8.12)–(8.14)].

[17] Note that all considered stress expressions for the viscous matrix (compare equations (9), (30), (38) and the one given by *Sridhar et al.* [2001]) exhibit the same relation between stress, matrix viscosity, perturbation wavelength, and layer deflection and that additional multipliers (such as F_{det} and F_{dd}) contain information on matrix thickness, viscosity variation, and boundary conditions at the layer-matrix boundary. The four stress expressions can be variously combined into (1) to simulate a number of different folding situations.

5. Applicability of the Ductile Rheology to Competent Layers on the Lithospheric Scale

[18] In this section we consider depth-dependent rheology for the competent layer, which may become essential on the lithospheric scale. The viscosity of the competent layer (i.e., the

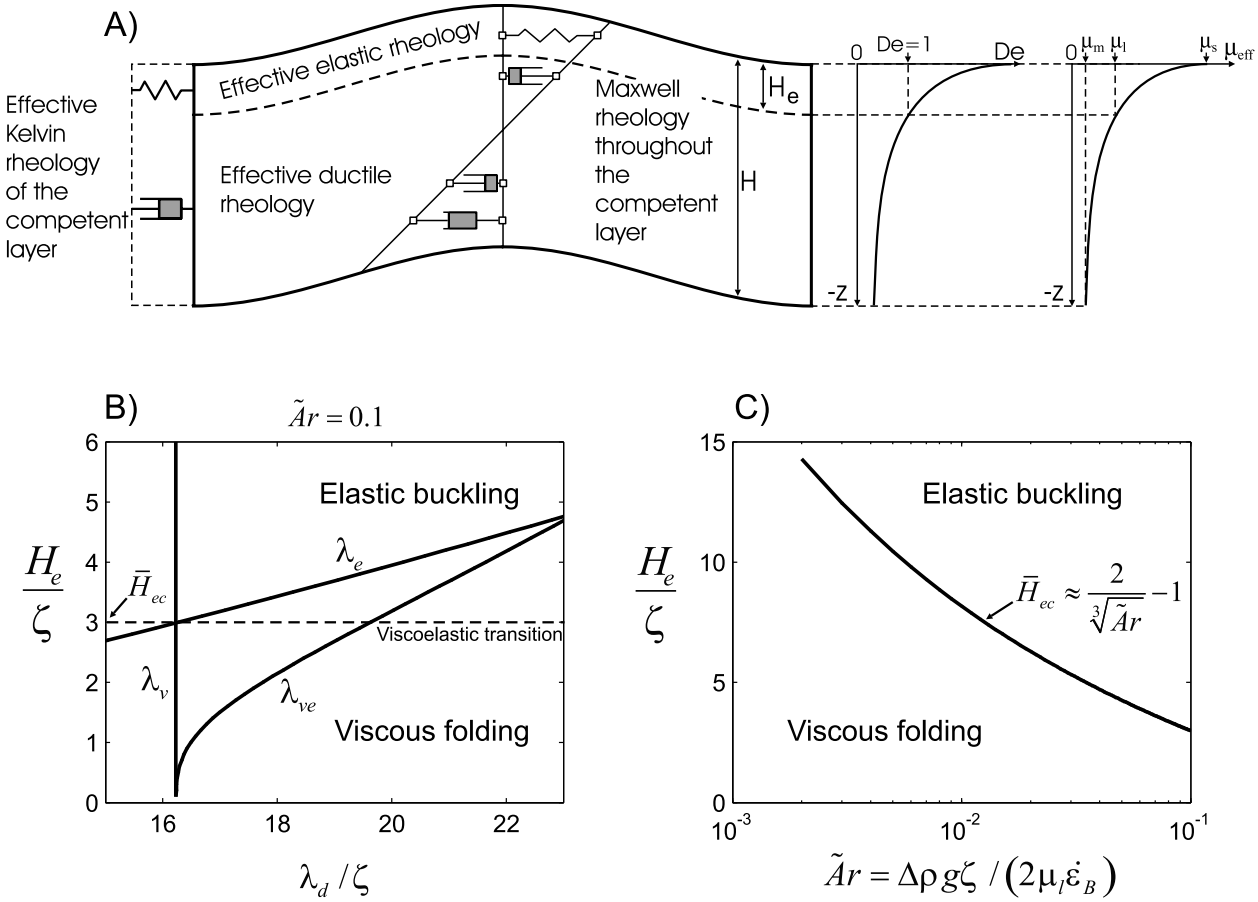

Figure 8. (a) The effective rheology of a folded, competent layer on the lithospheric scale. The rocks within the competent layer exhibit a Maxwell rheology (i.e., elastic and viscous element connected in series). At the lithospheric scale the temperature increases from around 0°C at the top of the competent layer to around 1300°C at the bottom. Owing to exponential temperature dependence, the viscosity and consequently the Deborah number ($De = \mu_{eff}\dot{\varepsilon}_B/G$) decrease exponentially with depth. The upper part of the competent layer with thickness H_e, in which $De > 1$, behaves quasi-elastic, whereas the lower part with thickness $H - H_e$ behaves quasi-viscous ($De < 1$). On the lithospheric scale the effective rheology of a competent layer consisting of rocks exhibiting a Maxwell rheology is the Kelvin rheology (elastic and viscous element connected in parallel). (b) Results for folding of a competent layer which consists of an elastic layer resting on top of a viscous layer with exponentially decreasing viscosity under the effects of gravity (see Figure 8a). The parameter λ_e is the dominant wavelength for folding if the viscous resistance is much smaller than the elastic, flexural resistance (i.e., elastic buckling), λ_v is the dominant wavelength for folding if the elastic, flexural resistance is much smaller than the viscous one (i.e., viscous folding), and λ_{ve} is the complete dominant wavelength solution for folding of the viscoelastic competent layer. For a critical value of H_e/ζ (designated as $\bar{H}_{ec}$), $\lambda_e = \lambda_v$. For values of $H_e/\zeta < \bar{H}_{ec}$, λ_{ve} is better approximated by λ_v than by λ_e and vice versa for $H_e/\zeta > \bar{H}_{ec}$. (c) $\bar{H}_{ec}$ only dependent on $\tilde{A}r$. The solid line separates the area where viscous folding is active from the one where elastic buckling is active.

lithosphere or the top crustal layer) is high, and its upward increase toward the Earth's surface may cause a switch in rheology from ductile to elastic in the upper part of the layer. The rheology of rocks is generally a combination of time-dependent (e.g., ductile) and time-independent (e.g., elastic) rheologies [e.g., *Turcotte and Schubert*, 1982; *Ranalli*, 1995], and competent layers on the lithospheric scale behave viscoelastically. Next we discuss conditions under which the elastic rheology can be neglected and whether the ductile rheology is sufficient to study lithospheric folding.

[19] The simplest rheological models describing viscoelastic behavior are the Maxwell body (elastic and viscous element connected in series) and the Kelvin body (elastic and viscous element connected in parallel) [e.g., *Findley et al.*, 1989]. For folding, *Schmalholz and Podladchikov* [2001a] demonstrated that viscoelastic layers behave either quasi-viscously or quasi-elastically depending on the single parameter R, which is a combination of the viscosity contrast between layer and matrix and the ratio of the layer-parallel stress to the layer's shear modulus. For $R >> 1$, layers with Kelvin rheology are quasi-viscous, whereas layers with Maxwell rheology are quasi-elastic, and vice versa for $R << 1$ [*Schmalholz and Podladchikov*, 2001a]. Therefore, to establish conditions under which viscoelastic layers on the lithospheric scale behave quasi-viscously (justifying the usage of ductile rheology), we must determine if their effective rheology is better approximated by the Kelvin model or the Maxwell model.

[20] In general, the effective rheology of rocks depends upon the loading mode. Isotropic compression by lithostatic pressure is better described by the Kelvin model (otherwise, rocks would suffer infinite compaction). In contrast, the response of rocks to shear loading, at any depth, is better described by the Maxwell model, which accounts for large shear strains and the relaxation of the elastic stresses. In this paper, we neglect the isotropic bulk

deformation, and rocks are thus considered incompressible. Then the Maxwell model is appropriate for the nonisotropic (deviatoric) deformation, but the situation is complicated by the temperature (depth) dependence of its viscous component. The Deborah number ($De = \mu_l \dot{\varepsilon}_B / G$ [e.g., *Reiner*, 1964]) is suitable for determining if viscoelastic rocks exhibiting a Maxwell rheology deform quasi-elastically ($De > 1$) or quasi-viscously ($De < 1$). The upper part of the competent layer may be nearly elastic at low temperatures ($De > 1$ for large values of μ_l), while the lower, high-temperature part is nearly viscous ($De < 1$ for small values of μ_l); that is, the overall response of the competent layer is Kelvin-type behavior (Figure 8a) [cf. *Schmalholz and Podladchikov*, 2001a]).

[21] Kelvin-type behavior can be simulated by a competent layer that consists of a thin elastic layer resting on top of a viscous layer with exponentially decreasing viscosity (compare equation (37) and Figure 8a). For such a competent layer we derived a solution using the perturbation method for the viscous sublayer using (28). Two boundary conditions are determined by assuming that the horizontal and vertical velocities are zero if the vertical coordinate $z \rightarrow -\infty$ (Figure 8a). The thin elastic sublayer is incorporated into the perturbation solution for the viscous sublayer through the boundary conditions. At the top of the viscous sublayer we set the remaining two boundary conditions for the stresses as

$$\sigma_{zz} = -2\mu_l \dot{\varepsilon}_B \left[\tilde{A}r \, \bar{W}(\bar{x}) - \frac{1}{6De} \left(\frac{H_e}{\zeta} \right)^3 \frac{\partial^4 \bar{W}(\bar{x})}{\partial \bar{x}^4} \right]$$
$$\tau_{xz} = -2\mu_l \dot{\varepsilon}_B \frac{\partial \bar{W}(\bar{x})}{\partial \bar{x}} \tag{47}$$

where $\tilde{A}r = \Delta\rho g \zeta / (2\mu_l \dot{\varepsilon}_B)$, H_e is the thickness of the elastic sublayer, ζ is the e-fold length of the viscosity variation, μ_l is the viscosity at the top of the viscous sublayer, and $W(\bar{x})$ is the dimensionless, vertical deflection of the elastic sublayer. We investigate the transition between quasi-viscous and quasi-elastic behavior and therefore set $De = 1$. Under layer-parallel compression the competent layer, consisting of both the elastic and viscous sublayer, buckles elastically if the flexural resistance of the elastic sublayer (controlled by $(H_e/\zeta)^3$) is dominant. Alternatively, the layer folds viscously if the elastic, flexural resistance is small compared to the viscous resistance. If the elastic and the viscous resistances are of the same order, the competent layer folds viscoelastically. The full dominant wavelength solution λ_{ve} for viscoelastic folding must include two end-member solutions: λ_e for elastic buckling under gravity with negligible viscous resistance [cf. *Turcotte and Schubert*, 1982], and λ_v for folding under gravity of a viscous half-space with exponentially decaying viscosity (equation (44) with $H = \zeta$ and $Ar = \tilde{A}r$). All three dominant wavelengths depend on $\tilde{A}r$, and for a given value of $\tilde{A}r$, there exists one value of H_e/ζ for which $\lambda_e = \lambda_v$ (Figure 8b). This critical elastic thickness which defines the viscoelastic transition is termed $\bar{H}_{ec}$. $\bar{H}_{ec}$ only depends on $\tilde{A}r$, and the relation between the two parameters is closely approximated by (Figure 8c)

$$\bar{H}_{ec} \approx \frac{2}{\sqrt[3]{\tilde{A}r}} - 1. \tag{48}$$

For $H_e/\zeta < \bar{H}_{ec}$ the competent layer folds viscously, but for $H_e/\zeta > \bar{H}_{ec}$ it buckles elastically.

[22] If estimates of $\tilde{A}r$ are available, (48) can be used to determine the critical elastic layer thickness. This thickness determines whether a competent layer consisting of an elastic layer resting on top of a viscous layer with exponentially decreasing viscosity folds in an elastic or viscous mode. Consequently, (48) can be used to estimate if the ductile rheology is applicable to competent layers on the lithospheric scale. Typical values for ζ for the ductile lithospheric mantle are around 2 km [see *Connolly and Podladchikov*, 1998, Figure 12], and for values of $0.01 < \tilde{A}r < 0.1$ the critical elastic thickness is around 3–7 times larger than ζ (compare Figure 8c), which provides a critical elastic thickness between 6 and 14 km.

6. Numerical Applications

[23] Folding is controlled by the effects of gravity if $S < 1$ and if the thickness of the matrix has a negligible influence. This means that (compare equation (14))

$$Ar > \frac{3}{2} \left(\frac{3n\mu_m}{\mu_{\text{eff}}} \right)^{\frac{2}{3}} \tag{49}$$

On the other hand, if the maximal amplification rate is smaller than the absolute value of the thickening rate due to background shortening (i.e., $\dot{\varepsilon}_B$), the deformation is dominantly accommodated by homogeneous layer thickening or inverse boudinage [cf. *Zuber*, 1987]. Therefore the ratio $\alpha_{\text{grav}}/\dot{\varepsilon}_B$ must be larger than one for folding to occur in the gravity-controlled mode. This means that from (20),

$$Ar < 6n. \tag{50}$$

Consequently, gravity-controlled folding only takes place for Argand numbers in the range of

$$\frac{3}{2} \left(\frac{3n\mu_m}{\mu_{\text{eff}}} \right)^{\frac{2}{3}} < Ar < 6n. \tag{51}$$

[24] The transition from matrix- to gravity-controlled folding occurs at $S = 1$. Solving (compare (14) with $S = 1$) for the layer thickness H yields a critical layer thickness:

$$H_{\text{crit}} = \frac{3\mu_{\text{eff}} \dot{\varepsilon}_B}{\Delta\rho g} \left(\frac{3n\mu_m}{\mu_{\text{eff}}} \right)^{\frac{2}{3}} \tag{52}$$

If a layer is thicker than H_{crit}, the effect of gravity must be included into calculations. Because of the simplifications made for deriving H_{crit}, the following examples are, of course, estimates of the exact value for the critical layer thickness. For example, using common values $\Delta\rho = 2500[\text{kg m}^{-3}]$, $g = 9.81[\text{m s}^{-2}]$, $\dot{\varepsilon}_B = 10^{-15}[\text{s}^{-1}]$, $n = 1$, $\mu_{\text{eff}} = 10^{22}[\text{Pa s}]$, and $\mu_m = 10^{19}[\text{Pa s}]$ yields ~25 m for H_{crit}. Keeping all above values fixed except $\mu_{\text{eff}} = 10^{21}[\text{Pa s}]$ yields $H_{\text{crit}} \approx 12$ m. For $\mu_{\text{eff}} = 10^{22}[\text{Pa s}]$ and $\mu_m = 10^{20}[\text{Pa s}]$ one gets $H_{\text{crit}} \approx 120$ m. According to these results, gravity starts to control folding if the layer thickness is larger than 10 to 100 m. However, H_{crit} strongly depends on μ_{eff} and the ratio of μ_m/μ_{eff}, which are the least constraint parameters. Therefore H_{crit} can be considerably smaller than 10 m if, for example, μ_{eff} is smaller than 10^{21}[Pa s] and μ_m/μ_{eff} is smaller than 0.001.

7. Geological Implications

[25] Our solution for folding with combined effects of gravity and matrix thickness (equation (32)) can be used to estimate the effective thickness of a strong, upper crust and a weaker, lower crust during crustal-scale folding. For example, a topographic wavelength of ~50 km is observed in central Asia, where the depth of the Moho is estimated to be ~50 km [*Burov et al.*, 1993]. The topographic wavelength is attributed to folding of a strong, upper crust resting on a weaker, ductile lower crust [*Burov et al.*, 1993]. The Moho is considered to be the top of a strong base (the upper mantle), and the upper crust is assumed to be decoupled from the upper mantle. However, to perform analytical investigations without considering gravity and matrix thickness, the effective thickness of the upper and lower crust and the effective viscosity contrast between the upper and lower crust have to be estimated a priori [*Burov et al.*, 1993]. Yet the only observable (i.e., measurable) parameter is the ratio of the topographic wavelength to the depth of the Moho. In a two-layer

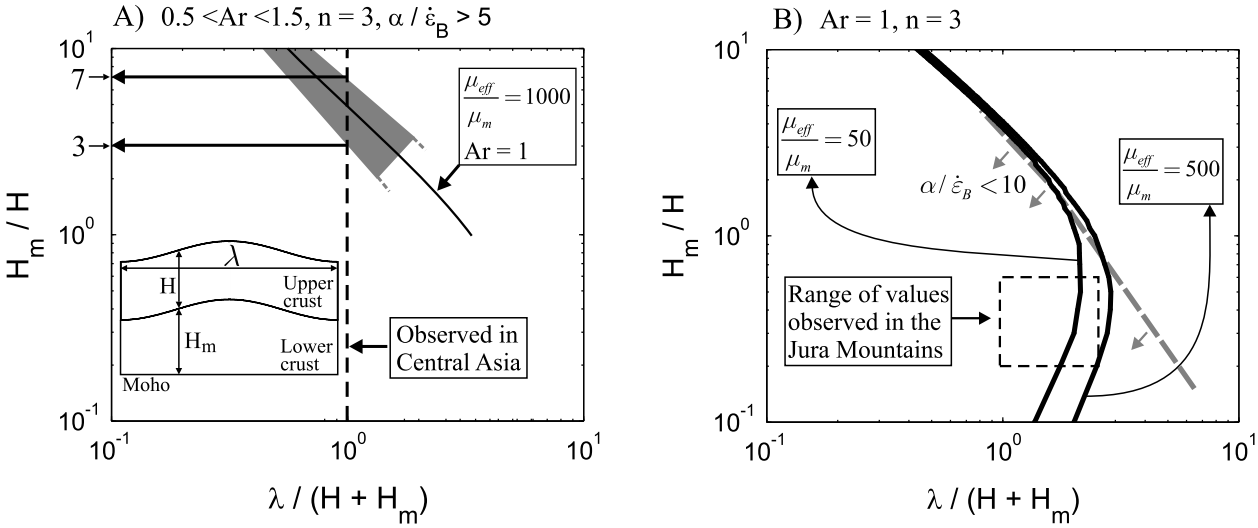

Figure 9. The ratio of dominant wavelength to total thickness ($\lambda/(H + H_m)$) versus the ratio of matrix thickness to layer thickness (H_m/H). (a) In central Asia both the observed topographic wavelength and the Moho depth (i.e., $H + H_m$) around 50 km, yielding $\lambda/(H + H_m) \approx 1$. For effective viscosity contrasts (μ_{eff}/μ_m) between 10 and 10,000 and Argand numbers (Ar) between 0.5 and 1.5, all results lie within the shaded field. The value of H_m/H is constrained between 3 and 7. (b) In the Jura Mountains, values of H_m/H between 0.2 and 0.6 and values of $\lambda/(H + H_m)$ between 1 and 2.5. The observed parameter range indicates that effective viscosity contrasts are smaller than ~500 and normalized amplification rates ($\alpha_{tot}/\dot{\varepsilon}_B$) are smaller than 10. This is also observed for Argand numbers between 0.5 and 1.5 and power law exponents (n) between 1 and 3.

model consisting of upper and lower crust the depth of the Moho is the sum of the thickness of the strong, upper crust (H) and the weak, lower crust (H_m). Using (32), the ratio of dominant wavelength to total thickness $\lambda/(H + H_m)$ can be plotted versus the ratio of matrix thickness to layer thickness H_m/H for different viscosity contrasts μ_{eff}/μ_m, (Figure 9a). This plot is done by taking the derivative of (32) with respect to $\bar{\omega}$, setting the derivative to zero and solving for the viscosity contrast which yields

$$\frac{\mu_{\text{eff}}}{\mu_m} = \frac{3n}{2}\frac{2\bar{\omega}^5\bar{H}_m^3 + 48\bar{\omega}^2 + Ar\left(\bar{\omega}^3\bar{H}_m^3 - 12\right)}{\bar{\omega}^6\bar{H}_m^3(\bar{\omega}^2 Ar)}, \qquad (53)$$

where $\bar{H}_m = H_m/H$. This viscosity contrast corresponds to the dominant wavelength. The ratio $\lambda/(H + H_m)$ can be introduced into (53) by the relation

$$\bar{\omega} = \frac{2\pi}{\frac{\lambda}{H+H_m}(1 + \bar{H}_m)} \qquad (54)$$

Equations (53) and (54) provide a relationship between the ratios of dominant wavelength to total thickness ($\lambda/(H + H_m)$), the ratio of matrix thickness to layer thickness (H_m/H), and the viscosity contrast (μ_{eff}/μ_m) for given values of Ar and n.

[26] To constrain the minimum value of Ar, we assume a typical power law exponent $n = 3$ and maximal viscous stresses, as defined by the brittle yield condition (see *Flesch et al.* [2001] for a detailed discussion). The Argand number is estimated by using a density of the lower crust of 2900 [kg m^{-3}] and replacing the denominator $2\mu_{eff}\dot{\varepsilon}_B$ by γH [*McAdoo and Sandwell*, 1985], where γ is the slope of Byerlee's law relating yield stress to depth. For a compressed crust, γ is $\sim 6 \times 10^4$ [Pa m^{-1}1] [*Byerlee*, 1978; *McAdoo and Sandwell*, 1985]. This γ value may overestimate the strength of the strong upper crust, and we vary γ between 6×10^4 [Pa m^{-1}] and 1.8×10^4 [Pa m^{-1}], which provides Argand numbers of ~0.5 and ~1.5, respectively. This range of Argand numbers is applicable to a broad spectrum of natural folding situations in which the folded layer rests on a weaker matrix. In our calculation we only considered dominant wavelengths that correspond to maximal amplification rates at least 5 times larger than the thickening rate (i.e., $\alpha_{tot}/\dot{\varepsilon}_B > 5$) because no significant fold amplitude will develop for smaller maximal amplification rates. The ratio of wavelength to total thickness (Moho depth) in central Asia is ~1. All results for viscosity contrasts ranging from 10 to 10,000 and Argand numbers between 0.5 and 1.5 cross the "observed" (i.e., constrained by available geophysical observations) line $\lambda/(H + H_m) = 1$ in a narrow band corresponding to values of H_m/H between 3 and 7 (Figure 9a). We see that without knowing the viscosity contrast and with only a rough approximation of the Argand number we can estimate the effective viscous thickness of the crust to be between 6.25 km ($H_m/H = 7$) and 12.5 km ($H_m/H = 3$). This yields ratios of wavelength to upper crustal thickness between 8 and 4, respectively. These values are similar to results of *Burov et al.* [1993], who estimated, from the matrix-controlled folding theory, the effective thickness of the upper crust between 10 and 15 km and the ratio of wavelength to upper crustal thickness between 4 and 6.

[27] A further application of our analytical solution has been made on the Jura Mountains, which are characterized by Mesozoic sediments dominated by limestones folded above a detachment zone within Triassic evaporites [*Buxtorf*, 1916; *Laubscher*, 1977; *Mosar*, 1999; *Sommaruga*, 1999]. We treat the foldedlimestones as a single layer and the Triassic as a homogeneous matrix with unknown effective viscosities. Using detailed sections [*Buxtorf*, 1916; *Laubscher*, 1977] provides average ratios of H_m/H between 0.2 and 0.6 and ratios of $\lambda/(H + H_m)$ between 1 and 2.5. Using (32) with the same range of Argand numbers as applied for central Asia (0.5–1.5) and standard power law exponents between 1 and 3 [*Turcotte and Schubert*, 1982] shows that the effective viscosity contrast is smaller than ~500 and that the ratio of amplification rate to shortening rate ($\alpha_{tot}/\dot{\varepsilon}_B$) is smaller than 10. Results are plotted for $Ar = 1$ and $n = 3$ (Figure 9b).

[28] Similarly, a considerable part of the Zagros mountains in southwest Iran, the so-called Simply Folded Belt [*Colman-Sadd*, 1978] consists of Paleozoic and Mesozoic sediments that were folded above a rigid basement on top of which Proterozoic sediments (Hormuz Series) acted as a detachment zone [*Bird*,

1978; *Colman-Sadd*, 1978; *Mann and Vita-Finzi*, 1988]. Folding is considered to have started in the Miocene, and therefore we ignore the sediments deposited since the Miocene because we analyze the initial wavelength selection process. These young sediments are, moreover, incompetent and exhibit much smaller-scale folds [*Colman-Sadd*, 1978]. Therefore the initial folding setup or geometry is the same as in central Asia and the Jura Mountains. Observed wavelengths in the Simply Folded Belt are between 6 and 18 km, the thickness of the folded series is between 6 and 7 km, and the thickness of the matrix (detachment zone) is between 1 and 1.5 km [*Colman-Sadd*, 1978; *Mann*, 1988]. Using the same range of Argand numbers and power law exponents as in the Jura Mountains indicates that in the Zagros Mountains the effective viscosity contrast was less than ~500, and the ratio of amplification rate to shortening rate was less than ~10.

8. Discussion and Conclusions

[29] In this study, linear stability analysis and thin-plate methods are used. The folded layer and the matrix exhibit homogeneous and isotropic material properties. Natural settings, especially on the crustal and lithospheric scales, are more complicated because of strong pressure and temperature dependence of material properties, complex rheologies, large strains, effects of shear heating, etc. Numerical methods are required to investigate large strain folding under more complex conditions [e.g., *Burov and Molnar*, 1998; *Burg and Podladchikov*, 1999; *Gerbault et al.*, 1999; *Schmalholz et al.*, 2001] because even powerful analytical methods, such as thick-plate or perturbation methods, are unsuitable to incorporate many complex natural conditions. This study does not investigate folding under lithospheric conditions but focuses on the simultaneously acting resistances due to gravity, matrix viscosity, and matrix thickness against fold amplification and especially on the transitions at which one of these resistances starts to control folding. For our purposes a simple analytical approach is advantageous because it allows the derivation of dimensionless parameters, such as S, that alone define the dominant wavelength and the transition between two different folding modes (Figure 3). S, for example, provides important information on how the involved physical parameters (e.g., H, μ_{eff}) affect folding. An increase in H causes S to decrease, which shifts folding closer to the gravity-controlled mode. Also, changing H has a stronger influence than a change in μ_{eff} because H appears with a larger absolute exponent in S than μ_{eff} (compare (14)). In addition, complex natural settings are usefully reduced to simpler settings with only a few layers characterized by so-called effective thicknesses and effective competence contrasts [e.g., *McAdoo and Sandwell*, 1985; *De Rito et al.*, 1986; *Burov and Diament*, 1995; *Zuber and Parmentier*, 1996]. This requires understanding of simplified folding processes such as the one considered in this study (Figure 1) and a posteriori justifies the application of simplified folding models to more complex, natural situations.

[30] The dominant wavelength for gravity-controlled folding of ductile layers (equation (18)) depends on the square root of the Argand number, a result at variance with the solution proposed by *Burov and Molnar* [1998] and *Cloetingh et al.* [1999], which depends on the fourth root of the Argand number. This discrepancy occurs because they employed the so-called equilibrium analysis [e.g., *Bazant and Cedolin*, 1991], which requires anapproximation of the inherently time-dependent viscous formulationby an effective quasi-static (e.g., elastic) model involving only stationary parameters (e.g., background strain rate $\dot{\varepsilon}_B$). To achieve this reduction, the kinematic equation (8) was approximated as

$$\dot{\varepsilon}_F = -z\frac{\partial^3 W(x,t)}{\partial x^2 \partial t} = -\alpha z \frac{\partial^2 W(x,t)}{\partial x^2} \approx -\dot{\varepsilon}_B z \frac{\partial^2 W(x,t)}{\partial x^2}, \quad (55)$$

which is equivalent to setting the folding growth rate equal to the background strain rate, i.e., $\alpha \approx \dot{\varepsilon}_B$. If the more accurate expression for $\alpha = 6n\dot{\varepsilon}_B/Ar$ (equation (20)) is used, the square root dependence of the buckling wavelength, λ_{crit}, on the Argand number is recovered within the framework of the equilibrium or "loss of stability" analysis [*Turcotte and Schubert*, 1982, equation (3–124)]:

$$\lambda_{crit} = 2\pi H \sqrt[4]{\frac{\alpha}{6\dot{\varepsilon}_B Ar}} = \frac{2\pi H \sqrt[4]{n}}{\sqrt{Ar}} \quad (56)$$

in agreement with (18) for the Newtonian case ($n = 1$). The fact that both solutions fit the observations of crustal folding in central Asia suggests that the Argand number is of order 1 and $\alpha \sim \dot{\varepsilon}_B$ for this particular case.

[31] We show that folding dominates homogeneous layer thickening if $Ar < Ar_{crit} = 6n$ (equation (50)). More accurate thick-plate analysis lowers Ar_{crit} to $\approx 2.5n$. Homogeneous (constant trough depth) layer thickening of the crust and lithosphere has been applied to model the Indian-Asian continental collision using the so-called thin viscous sheet model [*England and McKenzie*, 1982; *Houseman and England*, 1993]. In these models the Argand number is defined differently [*England and McKenzie*, 1982, equation (19)] than it is here (equation (13)) due to the different problem setup. We use the density difference between the material below and above the layer to characterize the gravitational stress and the background strain rate to describe the layer-parallel stress. *England and McKenzie* [1982] use the density contrast between the layer material, ρ_c, and the material below the layer, ρ_m, to describe the gravitational stress and the ratio of the indentation velocity, u_0, to layer thickness, H, to characterize the layer-parallel stress. In the following, the Argand number originally introduced for the thin sheet model is designated Ar^{TS} and, in our notation, is

$$Ar^{TS} = \frac{\rho_c}{\rho_m}\left(1 - \frac{\rho_c}{\rho_m}\right)\frac{\rho_m g H}{B(u_0/H)^{\frac{1}{n}}}. \quad (57)$$

Assuming a mantle density of 3300 [kg m^{-3}] and crustal density of 2725 [kg m^{-3}], the conversion between the two definitions is

$$Ar^{TS} \approx \frac{1}{7}\left(\frac{\dot{\varepsilon}_B}{u_0/H}\right)^{1/n} \quad Ar \approx \frac{1}{7}\left(\frac{H}{L}\right)^{\frac{1}{n}} Ar, \quad (58)$$

where our background shortening strain rate is replaced by the ratio of the indentation velocity to the characteristic horizontal length scale L of the deforming area, i.e., $\dot{\varepsilon}_B = u_0/L$. If $L \sim H$, then our Argand number is around 7 times larger than the one used in the thin viscous sheet models. The homogeneously thickening thin sheet model is appropriate if

$$Ar^{TS} \gg Ar^{TS}_{crit} = \frac{1}{7}\left(\frac{H}{L}\right)^{\frac{1}{n}} Ar_{crit} \approx \frac{n}{3}\left(\frac{H}{L}\right)^{\frac{1}{n}} \quad (59)$$

(using the thick-plate estimate $Ar_{crit} = 2.5n$). On the other hand, the Ar^{TS} number must be <10 to sustain appreciable crustal elevation contrasts [*England and McKenzie*, 1982]. *England and Houseman* [1986] found that the value of Ar^{TS} number that gives the best match to central Asian topography is ~1 if $n = 3$ and is ~3 if $n = 10$, and they focus on these two cases in subsequent publications [*Houseman and England*, 1993]. However, both sets of these parameters result in $Ar^{TS} \approx Ar^{TS}_{crit}$. This result means that for the values of the Argand number and n used by *Houseman and England* [1993], layer thickening is not the sole deformation mechanism: Folding provides maximal amplification rates that are of the same order as the thickening rates. In this case, the folding instability and the layer

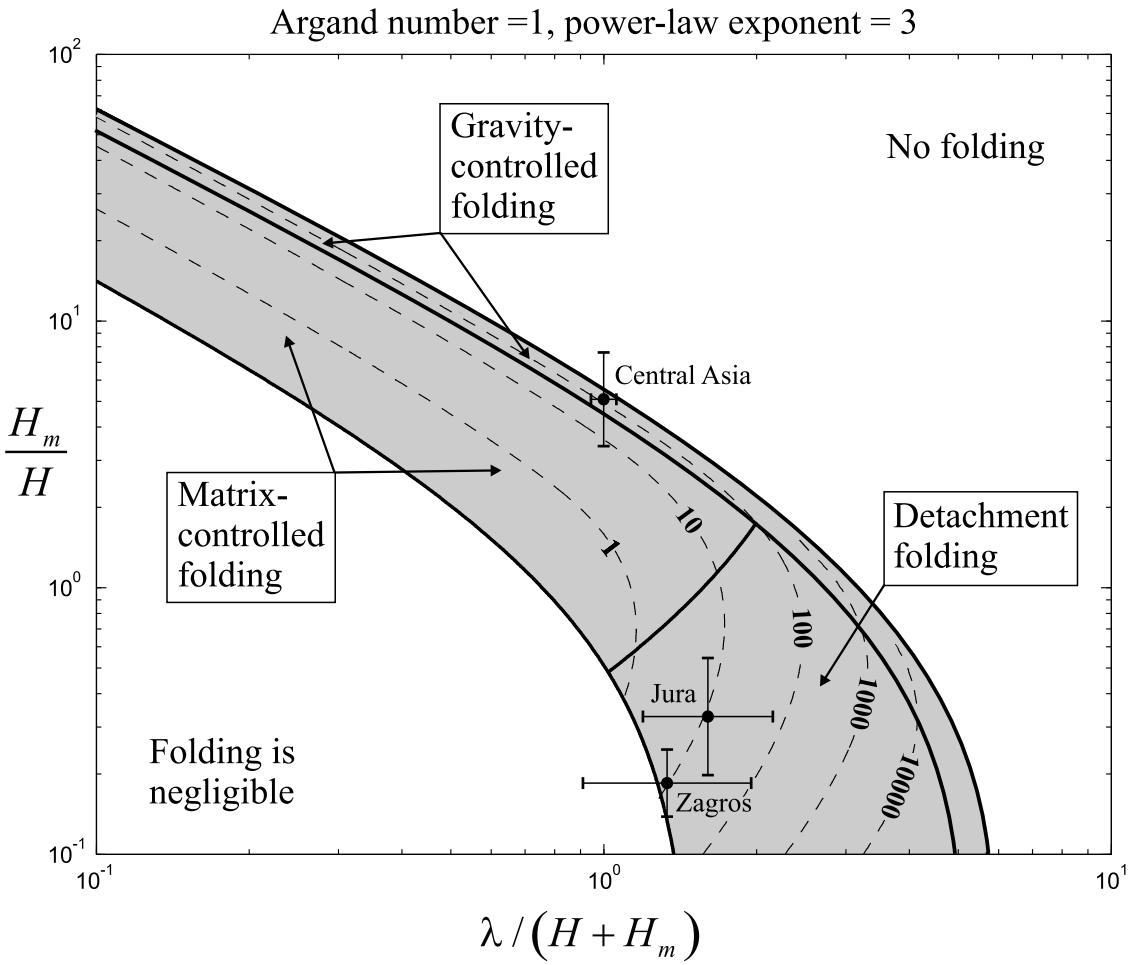

Figure 10. Phase diagram for fundamental folding modes for given values of the Argand number (Ar) and the power law exponent (n) of the layer material. The phase diagram is constructed using as coordinates the ratio of matrix thickness to layer thickness (H_m/H) and the ratio of wavelength to total thickness ($\lambda/(H + H_m)$). The dashed lines are contour lines of the effective viscosity contrast (μ_{eff}/μ_m is given by the numbers on the dashed lines) between layer and matrix. Folding is negligible if the maximal amplification rate of the folding instability is smaller than the thickening rate of the layer. The narrow field for gravity-controlled folding limits the fields for matrix-controlled and detachment folding because for fold geometries above the line for gravity-controlled folding, the amplification rates for matrix-controlled and detachment folding are larger than the one for gravity-controlled folding. The active folding mode is determined by the mode that provides the slowest amplification rate (see Figure 5).

thickening equally contribute to the uplift rates of the topography and neither mode can be neglected. We argue that the thin viscous sheet models (with either $n = 3$, $Ar^{TS} = 1$ or $n = 10$, $Ar^{TS} = 3$ and deformation simplified to be depth-independent) are accurate only in areas where the horizontal length scale of the deformed area is much larger than the thickness of the thin sheet. Although the length L is not known a priori in the thin viscous sheet models, it is hard to satisfy the applicability condition, $(L/H)^{1/n} \gg 1$, everywhere in the computational domain, especially if $n = 10$ is used (preferable for matching the degree of strain localization). Moreover, in the thin viscous sheet models of *Houseman and England* [1993] the horizontal length scale of the deformation at sides and corners of the indentation is much smaller than the horizontal length scale of the deformed area in the front of the indentation (as in Figures 3 and 4 of *Houseman and England* [1993]). The corners of the indentation, the so-called syntaxes, are the sites of high shortening strain rates orthogonal to the indentation direction. Arguably, syntaxes are the areas where folding dominates homogeneous thickening and the thin sheet approximations must be extended to handle folding [*Medvedev and Podladchikov*, 1999a, 1999b]. Large-scale folding as the primary response to shortening has indeed been suggested for both syntaxes of the Indian-Asian continental collision [*Burg and Podladchikov*, 1999].

[32] We show that the effective rheology of competent layers on the lithospheric scale can be described by the Kelvin rheology. This rheology may be suitable to describe the effective rheology of the oceanic lithosphere, especially in the context of the initial folding stages during compression. A shortened oceanic lithosphere would behave quasi-elastically, if the thickness of its elastic sublayer exceeds the limit given by (48). We speculate that on Earth this limit (~5–15 km) may be exceeded and the resulting quasi-elastic behavior of the oceanic lithosphere would explain its plate-like behavior ("memory" of the internal stress state and geometry). In contrast, the thickness of the top elastic layer may not exceed the critical value on Venus due to its high surface temperature explaining the absence of plate tectonics.

[33] The application of our analytical results to folding in central Asia and the Zagros and Jura Mountains shows the advantage of the geometrical parameter H_m because it allows the use of observable, geometrical information such as the ratio

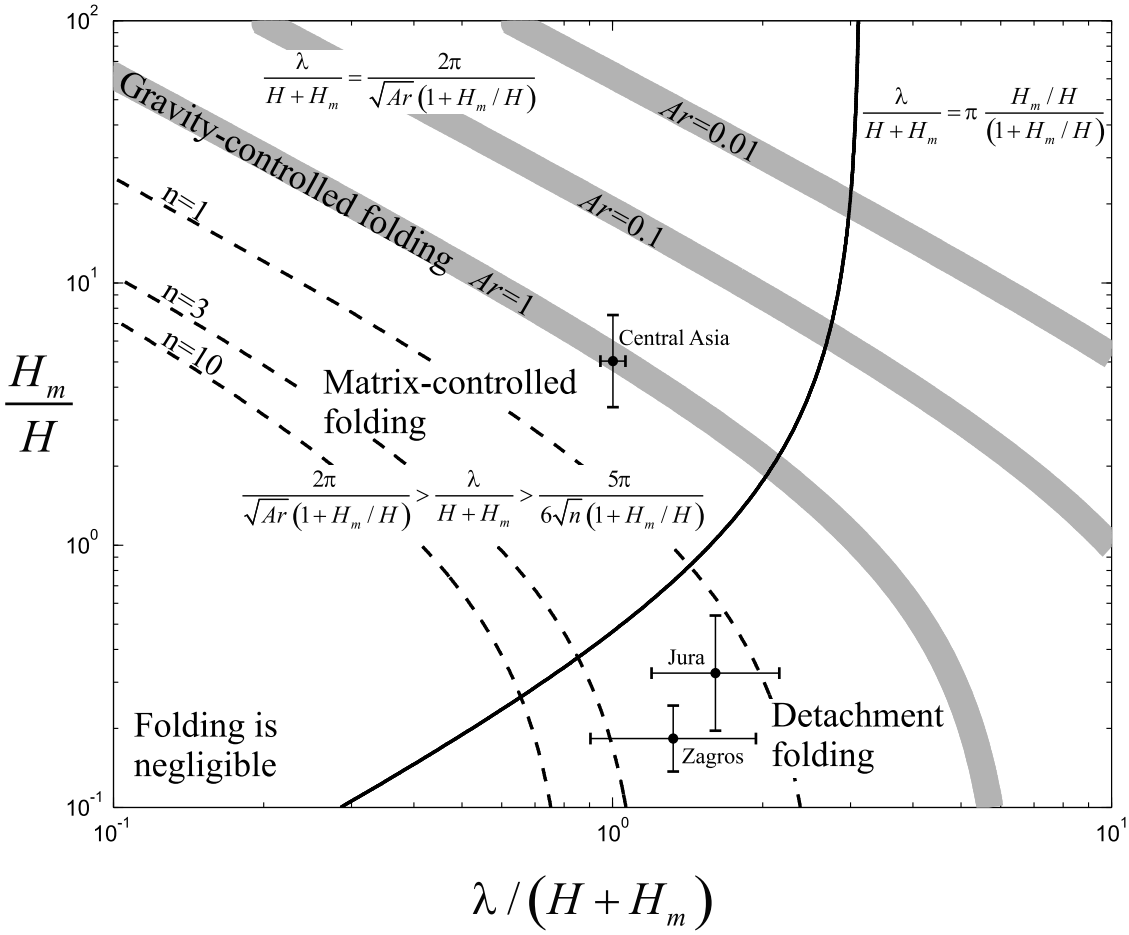

Figure 11. General phase diagram for fundamental folding modes. The phase diagram is constructed using as coordinates the ratio of matrix thickness to layer thickness (H_m/H) and the ratio of wavelength to total thickness ($\lambda/(H + H_m)$). The transition between matrix-controlled and detachment folding is defined by the single, solid line. The equation for this line only depends on $\lambda/(H + H_m)$ and H_m/H. The fields for matrix-controlled and detachment folding are bounded at their top by the shaded lines that define the gravity-controlled folding mode. The gravity-controlled folding mode only occurs within a narrow field. The thick shaded lines defining the gravity-controlled folding mode depend in addition on the coordinates of the phase diagram on the Argand number (Ar). A decrease in Ar causes an increase in the fields for the matrix-controlled and detachment folding mode. For example, for $Ar \approx 1$, folding in central Asia takes place in the gravity-controlled folding mode, but for $Ar << 1$, folding takes place in the matrix-controlled folding mode. These fields for the matrix-controlled and detachment folding mode are bounded at their bottom by the dashed lines, which represent the constraint that the maximal amplification rates must be larger than the layer thickening rate (i.e., $\alpha_{tot}/\dot{\varepsilon}_B > 1$). These boundary lines depend on the power law exponent (n), and increasing n increases the active fields for matrix-controlled and detachment folding. These lines show that for folding in the Jura and the Zagros Mountains, n must have been larger than 1.

of wavelength to total thickness $\lambda/(H + H_m)$ and the ratio of matrix thickness to layer thickness H_m/H. *Burov et al.* [1993] constrained the effective viscosity contrast between upper and lower crust to values between 20 and 30 in order to obtain ratios of crustal wavelength to crustal thickness λ/H between 4 and 6. However, our results, including gravity and matrix thickness, show that such values can be obtained for effective viscosity contrasts between 10 and 10,000. Therefore the ratio λ/H does not provide a reliable information about the effective viscosity contrast (see also Figure 10).

[34] The ratios $\lambda/(H + H_m)$ and H_m/H can be used to construct a phase diagram for the three folding modes (Figure 10). If the Argand number (Ar) and the power law exponent (n) are fixed, the three folding modes can be determined within the space $\lambda/(H + H_m) - H_m/H$. The critical maximal amplification rate ($\alpha_{tot}/\dot{\varepsilon}_B$), below which folding is considered to be negligible, is set to one. For folding with $\alpha_{tot}/\dot{\varepsilon}_B < 1$, no observable fold shapes will develop. The amplification rates within the matrix-controlled and the detachment folding mode depend on the viscosity contrast (dashed lines in Figure 10) where increasing viscosity contrasts cause increasing growth rates (compare equations (19) and (36)). In the matrix-controlled and detachment folding fields the contours of the effective viscosity contrast allows estimation of the effective viscosity contrast if estimates of the Argand number are available. The gravity-controlled folding mode is independent of the viscosity contrast (compare equation (20)) and is therefore represented by a line rather than a field within the space $\lambda/(H + H_m) - H_m/H$. More generally, the phase diagram can be constructed for variable values of Ar and n (Figure 11). The transition between matrix-controlled and detachment folding (the solid line in Figure 11) depends only on the ratios of $\lambda/(H + H_m)$ and H_m/H and is independent of Ar and n. The equation for this transition is derived by equating λ_{mat} and λ_{det} (compare equations (17) and (35)), using (54) and solving for $\lambda/(H + H_m)$. The

boundary at which the maximal amplification rates for matrix-controlled and detachment folding are equal to one (the dashed lines in Figure 11) depends on n. The analytical expression for this boundary is found by setting $\alpha_{mat} = 1$, using (54) and solving for $\lambda/(H + H_m)$. For folding geometries below the dashed lines, folding is negligible since $\alpha_{tot}/\dot{\varepsilon}_B < 1$. The line at which gravity-controlled folding is active can be constructed with (18) and (54).

[35] The phase diagram presented in Figure 11 provides implications for the observed folds in central Asia and the Jura and Zagros Mountains. For central Asia, Argand numbers cannot be considerably larger than 1 because folding cannot occur for the observed fold geometries. If Argand numbers are around 1, the folding in central Asia occurred in the gravity-controlled folding mode. If Argand numbers were considerably smaller than 1, the folding would occur in the matrix-controlled folding mode. Folding in the Jura and the Zagros Mountains took place in the detachment folding mode. Moreover, the power law exponents are required to be larger than 1 for folding to occur. It can be argued that the maximal amplification rates should be at least > 3 for noticeable fold shapes to develop, which would imply power law exponents larger than 5.

[36] The upper limits for the ratios of amplification rate to shortening rate estimated for the Jura and Zagros Mountains are around 10 (Figure 9b). These values are obtained by assuming that the observed fold wavelength corresponds to the dominant wavelength. However, the wavelength selected in the nucleation stage decreases with progressive shortening [*Sherwin and Chapple*, 1968], and observed wavelengths are smaller than the initial dominant wavelengths. Taking this effect into account, the values of $\lambda/(H + H_m)$ would increase and the observed fields, representing the geometry of the folds in central Asia and the Zagros and Jura Mountains, would move to larger values of $\lambda/(H + H_m)$, i.e., to the right in Figure 11. However, because of logarithmic axes of the phase diagrams, these results corrected for strain would not change the estimated folding mode but would increase the estimated limits for the ratios of amplification rate to shortening rate. Better estimates for these limits can be obtained by incorporating the change of wavelength and arc length during folding in the analytical theory [e.g., *Sherwin and Chapple*, 1968; *Schmalholz and Podladchikov*, 2000], which complicates the analytical results and requires additional information on strain [e.g., *Schmalholz and Podladchikov*, 2001b].

[37] According to our phase diagrams (Figures 5 and 11), folds can be assigned to different modes that provide different types of information: (1) Matrix-controlled folding provides information about the effective viscosity contrast between the folded layer and the matrix, (2) gravity-controlled folding provides information about the Argand number, and (3) detachment folding provides information about the thickness of the detachment zone (Table 1).

[38] Finally, it can be seen from Table 1 that for all folding modes (including folding with depth-dependent matrix viscosity (equation (42)), the same approximate relationship always exists between the maximum amplification rate, α_d, and the dominant wavelength, λ_d, namely,

$$\frac{\alpha_d}{\dot{\varepsilon}_B} \approx \frac{n}{\pi^2}\left(\frac{\lambda_d}{H}\right)^2. \qquad (60)$$

This means that a first-order estimate of the amplification rate can be done for any fold by only observing the ratio of wavelength to thickness and a rough estimation of the power law exponent of the layer material.

[39] **Acknowledgments.** We thank E. Burov, A. P. van den Berg, and C. Matyska for helpful and constructive reviews. We are grateful to D. Bernoulli for providing information about the Jura Mountains and to Dani Schmid for collaboration in deriving the thick-plate results. James Connolly is thanked for improving the English of the manuscript. S. M. Schmalholz was supported by ETH project 0-20-499-98.

References

Bassi, G., and J. Bonnin, Rheological modelling and deformation instability of lithosphere under extension, *Geophys. J.*, *93*, 485–504, 1988.

Bazant, Z. P., and L. Cedolin, *Stability of Structures: Elastic, Inelastic, Fracture, and Damage Theories*, Oxford Univ. Press, New York, 1991.

Biot, M. A., Theory of folding of stratified viscoelastic media and its implications in tectonics and orogenesis, *Geol. Soc. Am. Bull.*, *72*, 1595–1620, 1961.

Biot, M. A., *Mechanics of Incremental Deformations*, John Wiley, New York, 1965.

Bird, P., Finite element modeling of lithosphere deformation: The Zagros collision orogeny, *Tectonophysics*, *50*, 307–336, 1978.

Braun, J., and C. Beaumont, Styles of continental rifting: Results from dynamic models of lithospheric extension, in *Sedimentary Basins and Basin-Forming Mechanisms*, edited by C. Beaumont and A. J. Tankard, *Mem. Can. Soc. Pet. Geol.*, *12*, 241–258, 1987.

Burg, J.-P., and Y. Y. Podladchikov, Lithospheric scale folding: Numerical modelling and application to the Himalayan syntaxes, *Int. J. Earth Sci.*, *88*, 190–200, 1999.

Burov, E. B., and M. Diament, The effective elastic thickness (T_e) of continental lithosphere: What does it really mean?, *J. Geophys. Res.*, *100*, 3905–3927, 1995.

Burov, E. B., and P. Molnar, Gravity anomalies over the Ferghana Valley (central Asia) and intracontinental deformation, *J. Geophys. Res.*, *103*, 18,137–18,152, 1998.

Burov, E. B., L. I. Lobkovsky, S. A. P .L. Cloetingh, and A. M. Nikishin, Continental lithosphere folding in central Asia, part II, Constraints from gravity and topography, *Tectonophysics*, *226*, 73–87, 1993.

Buxtorf, A., Prognosen und Befunde beim Hauensteinbasis- und Grenchenbergtunnel und die Bedeutung der letzteren für die Geologie des Juragebirges, *Verh. Naturforsch. Ges. Basel*, *27*, 185–254, 1916.

Byerlee, E. B., Friction of rocks, *Pure Appl. Geophys.*, *116*, 615–626, 1978.

Chapple, W. M., A mathematical theory of finite amplitude rock folding, *Geol. Soc. Am. Bull.*, *79*, 47–68, 1968.

Cloetingh, S. A. P. L., E. Burov, and A. Poliakov, Lithosphere folding: Primary response to compression? (from central Asia to Paris Basin), *Tectonics*, *18*, 1064–1083, 1999.

Colman-Sadd, S. P., Fold development in Zagros simply folded belt, southwest Iran, *AAPG Bull.*, *62*, 984–1003, 1978.

Connolly, J. A. D., and Y. Y. Podladchikov, Compaction-driven fluid flow in viscoelastic rock, *Geodyn. Acta*, *11*, 55–84, 1998.

Currie, I. B., H. W. Patnode, and R. P. Trump, Development of folds in sedimentary strata, *Geol. Soc. Am. Bull.*, *73*, 655–674, 1962.

De Rito, R. F., F. A. Cozzarelli, and D. S. Hodge, A forward approach to the problem of nonlinear viscoelasticity and the thickness of the mechanical lithosphere, *J. Geophys. Res.*, *91*, 8295–8313, 1986.

Drazin, P. G., and W. H. Reid, *Hydrodynamic Stability*, Cambridge Univ. Press, New York, 1981.

England, P., and G. Houseman, Finite strain calculations of continental deformation, 2, Comparison with Indian-Asia collision zone, *J. Geophys. Res.*, *91*, 3664–3676, 1986.

England, P., and D. McKenzie, A thin viscous sheet model for continental deformation, *Geophys. J. R. Astron. Soc.*, *70*, 295–321, 1982.

Epard, J. L., and R. H. Groshong, Kinematic model of detachment folding including limb rotation, fixed hinges and layer-parallel strain, *Tectonophysics*, *247*, 85–103, 1995.

Findley, W. N., J. S. Lai, and K. Onaran, *Creep and Relaxation of Nonlinear Viscoelastic Materials*, Dover, Mineola, N. Y., 1989.

Flesch, L. M., A. J. Haines, and W. E. Holt, Dynamics of the Indian-Eurasia collision zone, *J. Geophys. Res.*, *106*, 16,435–16,460, 2001.

Fletcher, R. C., Wavelength selection in the folding of a single layer with power-law rheology, *Am. J. Sci.*, *274*, 1029–1043, 1974.

Fletcher, R. C., and B. Hallet, Unstable extension of the lithosphere: A mechanical model for Basin-and-Range structure, *J. Geophys. Res.*, *88*, 7457–7466, 1983.

Gerbault, M., E. Burov, A. N. B. Poliakov, and M. Daignieres, Do faults trigger folding in the lithosphere?, *Geophys. Res. Lett.*, *26*, 271–274, 1999.

Goff, D. F., D. V. Wiltschko, and R .C. Fletcher, Décollement folding as a mechanism for thrust-ramp spacing, *J. Geophys. Res.*, *101*, 11,341–11,352, 1996.

Houseman, G., and P. England, Crustal thickening versus lateral expulsion in the Indian-Asian continental collision, *J. Geophys. Res.*, *98*, 12,233–12,249, 1993.

Hunt, G., H. Mühlhaus, B. Hobbs, and A. Ord, Localized folding of viscoelastic layers, *Geol. Rundsch.*, *85*, 58–64, 1996.

Johnson, A. M., Folding and faulting of strain-hardening sedimentary rocks, *Tectonophysics*, *62*, 251–278, 1980.
Johnson, A. M., and R. C. Fletcher, *Folding of Viscous Layers*, Columbia Univ. Press, New York, 1994.
Laubscher, H., Fold development in the Jura, *Tectonophysics*, *37*, 337–362, 1977.
Lin, C. C., and L. A. Segel, *Mathematics Applied to Deterministic Problems in the Natural Sciences*, Macmillan, Old Tappan, N. J., 1974.
Mann, C. D., and C. Vita-Finzi, Holocene serial folding in the Zagros, in *Gondwana and Tethys*, edited by M. G. Audley-Charles and A. Hallam, pp. 51–59, Oxford Univ. Press, New York, 1988.
Martinod, J., and P. Davy, Periodic instabilities during compression or extension of the lithosphere, 1, Deformation modes from an analytical perturbation method, *J. Geophys. Res.*, *97*, 1999–2014, 1992.
Mase, G. E., *Continuum Mechanics*, McGraw-Hill, New York, 1970.
McAdoo, D. C., and D. T. Sandwell, Folding of oceanic lithosphere, *J. Geophys. Res.*, *90*, 8563–8569, 1985.
Medvedev, S. E., and Y. Y. Podladchikov, New extended thin-sheet approximation for geodynamic applications, I, Model formulation, *Geophys. J. Int.*, *136*, 567–585, 1999a.
Medvedev, S. E., and Y. Y. Podladchikov, New extended thin-sheet approximation for geodynamic applications, II, Two-dimensional examples, *Geophys. J. Int.*, *136*, 586–608, 1999b.
Mosar, J., Present-day and future tectonic underplating in the western Swiss Alps: Reconciliation of basement/wrench faulting and décollement folding of the Jura and Molasse basin in the Alpine foreland, *Earth Planet. Sci. Lett.*, *173*, 143–155, 1999.
Poblet, J., and K. McClay, Geometry and kinematics of single-layer detachment folds, *AAPG Bull.*, *80*, 1085–1109, 1996.
Ramberg, H., Fluid dynamics of viscous buckling applicable to folding of layererd rocks, *Am. Assoc. Pet. Geol. Bull.*, *47*, 484–505, 1963.
Ramberg, H., *Gravity, Deformation and the Earth's Crust*, Academic, San Diego, Calif., 1981.
Ramberg, H., and O. Stephansson, Compression of floating elastic and viscous plates affected by gravity, a basis for discussion crustal buckling, *Tectonophysics*, *1*, 101–120, 1964.
Ramsay, J. G., and M. I. Huber, *The Techniques of Modern Structural Geology*, vol. 2, *Folds and Fractures*, Academic, San Diego, Calif., 1987.
Ranalli, G., *Rheology of the Earth*, Chapman and Hall, New York, 1995.
Reddy, J. N., *Theory and Analysis of Elastic Plates*, Taylor and Francis, Philadelphia, Pa., 1999.
Reiner, M., The Deborah number, *Phys. Today*, *17*, 62, 1964.
Ricard, Y., and C. Froidevaux, Stretching instabilities and lithospheric boudinage, *J. Geophys. Res.*, *91*, 8314–8324, 1986.
Schmalholz, S. M., and Y. Y. Podladchikov, Buckling versus folding: Importance of viscoelasticity, *Geophys. Res. Lett.*, *26*, 2641–2644, 1999.
Schmalholz, S. M., and Y. Y. Podladchikov, Finite amplitude folding: Transition from exponential to layer length controlled growth, *Earth Planet. Sci. Lett.*, *181*, 619–633, 2000.
Schmalholz, S. M., and Y. Y. Podladchikov, Viscoelastic folding: Maxwell versus Kelvin rheology, *Geophys. Res. Lett.*, *28*, 1835–1838, 2001a.
Schmalholz, S. M., and Y. Y. Podladchikov, Strain and competence contrast estimation from fold shape, *Tectonophysics*, *340*(3–4), 195–213, 2001b.
Schmalholz, S. M., Y. Y. Podladchikov, and D. W. Schmid, A spectral/finite difference method for simulating large deformations of heterogeneous, viscoelastic materials, *Geophys. J. Int.*, *145*, 199–208, 2001.
Shen, F., L. H. Royden, and B. C. Burchfiel, Large-scale crustal deformation of the Tibetan Plateau, *J. Geophys. Res.*, *106*, 6793–6816, 2001.
Sherwin, J., and W. M. Chapple, Wavelengths of single layer folds: A comparison between theory and observation, *Am. J. Sci.*, *266*, 167–179, 1968.
Smith, R. B., Formation of folds, boudinage, and mullions in non-Newtonian materials, *Geol. Soc. Am. Bull.*, *88*, 312–320, 1977.
Sommaruga, A., Décollement tectonics in the Jura foreland fold-and-thrust belt, *Mar. Pet. Geol.*, *99*, 111–134, 1999.
Sridhar, N., D. J. Srolovitz, and Z. Suo, Kinetics of buckling of a compressed film on a viscous substrate, *Appl. Phys. Lett.*, *78*, 2482–2484, 2001.
Timoshenko, S. P., and S. Woinowsky-Krieger, *Theory of Plates and Shells*, McGraw-Hill, New York, 1959.
Turcotte, D. L., and G. Schubert, *Geodynamics: Applications of Continuum Physics to Geological Problems*, John Wiley, New York, 1982.
Twiss, R. J., and E. M. Moores, *Structural Geology*, W. H. Freeman, New York, 1992.
Whitten, E. H. T., *Structural Geology of Folded Rocks*, Rand McNally, Chicago, Ill., 1966.
Zuber, M. T., Compression of oceanic lithosphere: An analysis of intraplate deformation in the Central Indian Basin, *J. Geophys. Res.*, *92*, 4817–4825, 1987.
Zuber, M. T., and E. M. Parmentier, Finite amplitude folding of a continuously viscosity-stratified lithosphere, *J. Geophys. Res.*, *101*, 5489–5498, 1996.

J.-P. Burg, Geologisches Institut and Universität Zürich, ETH Zentrum, CH-8092 Zürich, Switzerland. (jpb@erdw.ethz.ch)
Y. Y. Podladchikov, Geologisches Institut, ETH Zentrum, CH-8092 Zürich, Switzerland. (yura@erdw.ethz.ch)
S. M. Schmalholz, Geomodelling Solutions GmbH, Binzstrasse 18, CH-8045 Zürich, Switzerland. (stefan.schmalholz@geomodsol.com)